NEW APPROACHES TO PULSE COMPRESSION TECHNIQUES OF PHASE-CODED WAVEFORMS IN RADAR

A THESIS SUBMITTED IN PARTIAL FULFILLMENT

OF THE REQUIREMENTS FOR THE DEGREE OF

Master of Technology

In

Telematics and Signal Processing

By

ANANGI SAILAJA

Roll No: 208EC108

Department of Electronics & Communication Engineering

National Institute of Technology

Rourkela

2010

NEW APPROACHES TO PULSE COMPRESSION TECHNIQUES OF PHASE-CODED WAVEFORMS IN RADAR

A THESIS SUBMITTED IN PARTIAL FULFILLMENT

OF THE REQUIREMENTS FOR THE DEGREE OF

Master of Technology

In

Telematics and Signal Processing

By

ANANGI SAILAJA

Roll No: 208EC108

Under the guidance of

Prof. AJIT KUMAR SAHOO

Department of Electronics & Communication Engineering

National Institute of Technology

Rourkela

2010

Dedicated to my family, my teachers,

my friends and all my well-wishers

National Institute Of Technology
Rourkela

CERTIFICATE

This is to certify that the thesis entitled, "**NEW APPROACHES TO PULSE COMPRESSION TECHNIQUES OF PHASE-CODED WAVEFORMS IN RADAR "** submitted by **ANANGI SAILAJA (208EC108)** in partial fulfillment of the requirements for the award of Master of Technology degree in Electronics and Communication Engineering with specialization in "Telematics and Signal Processing" during session 2009-2010 at National Institute of Technology, Rourkela (Deemed University) and is an authentic work by her under my supervision and guidance .

To the best of my knowledge, the matter embodied in the thesis has not been submitted to any other university/institute for the award of any Degree or Diploma.

Date:

Prof. Ajit Kumar Sahoo
Dept. of Electronics & Communication Engg.
National Institute of Technology
Rourkela-769008
Orissa, India

Acknowledgment

I would like to express my deep sense of respect and gratitude towards my advisor and guide **Prof. Ajit Kumar Sahoo,** who has been the guiding force behind this work. I want to thank him for introducing me to the field of Signal Processing and giving me the opportunity to work under him. I extend my sincere thanks and respects to **Prof. G.Panda** for his inspiration, tremendous help, advice and encouragement. I consider it my good fortune to have got an opportunity to work with such a wonderful person.

I express my respects to Prof. S.K. Patra, Prof. K.K. Mahapatra, Prof. G. S. Rath, Prof. S. Meher, Prof. S.K.Behera, Prof. Poonam Singh, Prof. D.P.Acharya, for teaching me and also helping me how to learn. They have been great sources of inspiration to me and I thank them from the bottom of my heart.

I would like to thank all faculty members and staff of the Department of Electronics and Communication Engineering, N.I.T. Rourkela for their generous help in various ways for the completion of this thesis.

Iam very thankful to my senior **Vikas Baghel**, who helped me a lot during my research work. I would like to thank all the Ph.D. scholars in DSP lab, my seniors and my friends especially Sunayana, Kranthi, Maitrayee, Sheema, Suresh, Chandu, Hanuma, Bharat, Shreeshail, Gyan, and Pyagyan for their help during the course of this work. I am also thankful to my classmates for all the thoughtful and mind stimulating discussions we had, which prompted us to think beyond the obvious.

I am especially indebted to my parents (Mr. A. Kuppi Reddy, Mrs E. Amaravathi), uncle, sisters and brothers-in-law for their love, sacrifice, and support. They are my first teachers after I came to this world and have set great examples for me about how to live, study, and work.

Anangi Sailaja

CONTENTS

ABSTRACT

The present thesis aims to make an in-depth study of Radar pulse compression, Neural Networks and Phase Coded pulse compression codes. Pulse compression is a method which combines the high energy of a longer pulse width with the high resolution of a narrow pulse width. The major aspects that are considered for a pulse compression technique are signal to sidelobe ratio (SSR) performance, noise performance and Doppler shift performance. Matched filtering of biphase coded radar signals create unwanted sidelobes which may mask important information. The adaptive filtering techniques like Least Mean Square (LMS), Recursive Least Squares (RLS), and modified RLS algorithms are used for pulse radar detection and the results are compared.

In this thesis, a novel approach for pulse compression using Recurrent Neural Network (RNN) is proposed. The 13-bit and 35-bit barker codes are used as signal codes to RNN and results are compared with Multilayer Perceptron (MLP) network. RNN yields better signal-to-sidelobe ratio (SSR), error convergence speed, noise performance, range resolution ability and doppler shift performance than neural network (NN) and some traditional algorithms like auto correlation function(ACF) algorithm. But the SSR obtained from RNN is less for most of the applications. Hence a Radial Basis Function (RBF) neural network is implemented which yields better convergence speed, higher SSRs in adverse situations of noise and better robustness in Doppler shift tolerance than MLP and ACF algorithm. There is a scope of further improvement in performance in terms of SSR, error convergence speed, and doppler shift. A novel approach using Recurrent RBF is proposed for pulse radar detection, and the results are compared with RBF, MLP and ACF. Biphase codes, namely barker codes are used as inputs to all these neural networks. The disadvantages of biphase codes include high sidelobes and poor Doppler tolerance.

The Golay complementary codes have zero sidelobes but they are poor Doppler tolerant as that of biphase codes. The polyphase codes have low sidelobes and are more Doppler tolerant than biphase codes. The polyphase codes namely Frank, P1, P2, P3, P4 codes are described in detail and autocorrelation outputs, phase values and their Doppler properties are discussed and compared. The sidelobe reduction techniques such as single Two Sample Sliding Window Adder(TSSWA) and double TSSWA after the autocorrelator output are discussed and their performances for P4 code are presented and compared. Weighting

techniques can also be applied to substantially reduce the range time sidelobes. The weighting functions such as Kaiser-Bessel amplitude weighting function and classical amplitude weighting functions (i.e. Hamming window) are described and are applied to the receiver waveform of 100 element P4 code and the autocorrelation outputs, Peak Sidelobe Level (PSL), Integrated Sidelobe Level (ISL) values are compared with that of rectangular window. The effects of weighting on the Doppler performance of the P4 code are presented and compared.

Keywords

Radar Pulse Compression, LMS, RLS, Modified RLS, MLP, RNN, RBF, RRBF, Golay complementary codes, Polyphase codes, TSSWA, Kaiser Bessel window, Hamming window.

LIST OF FIGURES

Page No.

LIST OF TABLES

Page No.

Acronyms

RADAR - Radio Detection And Ranging

ACF - Auto-Correlation Function

FIR - Finite Impulse Response

LMS - Least Mean Square

RLS - Recursive Least Squares

SNR - Signal to Noise Ratio

SSR - Signal to Sidelobe Ratio

ANN - Artificial Neural Network

MLP - Multi Layered Perceptron

RNN - Recurrent Neural Network

IMR - Input Magnitude Ratio

RBFNN - Radial Basis Function Neural Network

RRBF - Recurrent Radial Basis Function

TSSWA - Two Sample Sliding Window Adder

PSL - Peak Sidelobe Level

ISL - Integrated Sidelobe Level

K-B - Kaiser Bessel

Chapter – 1

Introduction

1.1. Background

RADAR is an acronym of Radio Detection And Ranging. There was a rapid growth in radar technology and systems during world war II. In the recent years, there were many accomplishments in radar technology. The major areas of radar applications includes military, remote sensing, air traffic control, law enforcement and highway safety, aircraft safety and navigation, ship safety and space [1.1, 1.2].

The rapid advances in digital technology made many theoretical capabilities practical with digital signal processing and digital data processing. Radar signal processing is defined as the manipulation of the received signal, represented in digital format, to extract the desired information whilst rejecting unwanted signals. Pulse compression allowed the use of long waveforms to obtain high energy simultaneously achieve the resolution of a short pulse by internal modulation of the long pulse. The resolution is the ability of radar to distinguish targets that are closely spaced together in either range or bearing. The internal modulation may be binary phase coding, polyphase coding, frequency modulation, and frequency stepping. There are many advantages of using pulse compression techniques in the radar field. They include reduction of peak power, relevant reduction of high voltages in radar transmitter, protection against detection by radar detectors, significant improvement of range resolution, relevant reduction in clutter troubles and protection against jamming coming from spread spectrum action [1.3].

In pulse compression technique, the transmitted signal is frequency or phase modulated (but not amplitude modulated) and the received signal is processed in the receiver, into a specific filter called "matched filter". In 1950-60, the practical realization of radars using pulse compression have taken place. At the starting, the realization of matched filters was difficult using traverse filters because of lack of delay line with enough bandwidth. Later matched filters have been realized by using dispersive networks made with lumped-constant filters. In recent years, instead of matched filters, many sophisticated filters are in use.

Barker code is the binary phase-coded sequence of 0, π values that result in equal side-lobes after passes through the matched filter. J.S.Fu and Xin wu proposed adaptive filtering techniques using LMS and RLS algorithms to suppress the sidelobes of barker code of length 13 [1.4]. The SSR and doppler performance of this type of filters are very poor. B.Zrnic et,al. proposed a self –clutter suppression filter design using modified RLS algorithm that gave better performance compared to iterative RLS and ACF algorithms [1.5].

A multilayered neural network approach using back propagation algorithm which yielded better SSR than basic ACF approach was presented by Kwan and Lee [1.6]. Khairnar et,al. [1.7] proposed a RBFN for pulse compression that yielded high SSRs in different adverse situations of noise, with misalignment of clock. This approach also has better range resolution and robustness in doppler shift interference. Frank proposed a polyphase code called as Frank code which is more Doppler tolerant and has lower sidelobes than binary codes [1.8]. Kretschmer and Lewis have presented the variants of Frank polyphase codes, namely P1, P2, P3, and P4 that have better properties than Frank code [1.9, 1.10].

1.2. Motivation

The pulse compression in radar has major applications in the recent years. For better pulse compression, peak signal to sidelobe ratio should be as high as possible so that the unwanted clutter gets suppressed and should be very tolerant under Doppler shift conditions. Many pulse compression techniques have come into existence including neural networks. The recurrent networks have inherent memory for dynamics that makes them suitable for dynamic system modelling. They provide better stability, more robust to estimation errors and good performance with more past information relevant to prediction. Hence the recurrent connections are applied to the MLP and RBF networks for pulse radar detection to achieve overall better performance. The study of polyphase codes and their sidelobe reduction techniques are carried out since the polyphase codes have low sidelobes and are better Doppler tolerant and better tolerant to precompression bandlimiting.

1.3. Thesis Organization

Chapter-1 Introduction

Chapter-2 Adaptive Filtering Techniques for Pulse radar Detection

The concept of pulse compression in radar is described in detail. The adaptive filtering techniques using LMS, RLS and modified RLS algorithms are discussed for pulse compression and the results are compared.

Chapter-3 Recurrent Neural Network Approach for Pulse Radar Detection

This chapter presents a novel recurrent neural network based pulse radar detection. The simulation results are compared with that of MLP and ACF algorithms.

Chapter-4 Recurrent RBF Approach for Pulse Radar Detection

This chapter proposes a novel recurrent RBF network based pulse radar detection technique which provides significant improvement in convergence rate, noisy conditions and under Doppler conditions. The proposed network is compared with the other networks like RNN, MLP and ACF.

Chapter-5 A Study of Polyphase Codes and their Sidelobe Reduction techniques

This chapter deals with the different polyphase codes such as Frank, P1, P2, P3, P4 and complementary codes namely Golay complementary codes. The study of these codes and their properties, sidelobe reduction techniques are carried out.

Chapter-6 Conclusion and Scope for Future Work

The concluding remarks for all the chapters is presented in this chapter. It also contains some future research topics which need attention and further investigation.

Chapter – 2

Adaptive Filtering Techniques For Pulse Radar Detection

2.1. Introduction

Radar is an electromagnetic system for detection and location of reflecting objects such as aircraft, ships, spacecraft, vehicles, people and natural environment [2.1]. It operates by radiating energy into space and detecting the echo signal reflected from object or target. The reflected energy that is returned to the radar not only indicates the presence of the target, but by comparing the received echo signal with the signal that was transmitted, its location can be determined along with other target-related information.

The basic principle of radar is simple. A transmitter generates an electro-magnetic signal (such as a short pulse of sine wave) that is radiated into space by an antenna. A portion of the transmitted signal is intercepted by a reflecting object (target) and is re-radiated in all directions. It is the energy re-radiated in back direction that is of prime interest to the radar. The receiving antenna collects the returned energy and delivers it to a receiver, where it is processed to detect the presence of the target and to extract its location and relative velocity. The distance to the target is determined by measuring the time taken for the radar signal to travel to the target and back. The range is

$$R = \frac{cT_R}{2} \tag{2.1}$$

where T_R is the time taken by the pulse to travel to target and return, c is the speed of propagation of electromagnetic energy (speed of light). Radar provides the good range resolution as well as long detection of the target.

The most common radar signal or waveform, is a series of short duration, somewhat rectangular-shaped pulses modulating a sinewave carrier [2.2]. Short pulses are better for range resolution, but contradict with energy, long range detection, carrier frequency and SNR. Long pulses are better for signal reception, but contradict with range resolution and minimum range. At the transmitter, the signal has relatively small amplitude for ease to generate and is large in time to ensure enough energy in the signal as shown in Figure 2.1. At the receiver, the signal has very high amplitude to be detected and is small in time [2.5].

A very long pulse is needed for some long-range radar to achieve sufficient energy to detect small targets at long range. But long pulse has poor resolution in the range dimension.

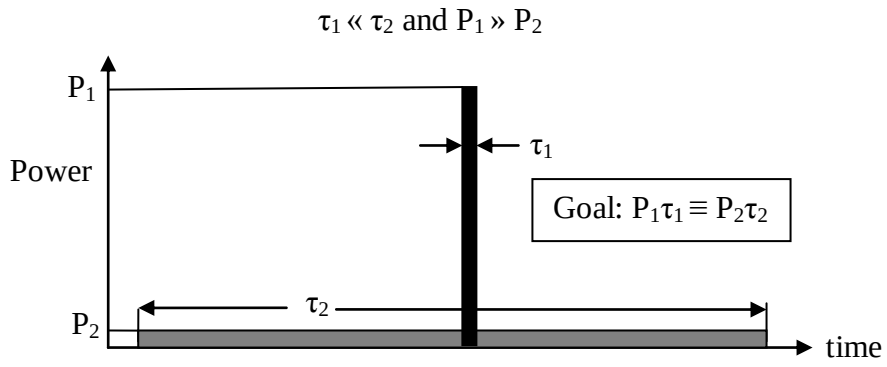

Figure 2.1. Transmitter and receiver ultimate signals

Frequency or phase modulation can be used to increase the spectral width of a long pulse to obtain the resolution of a short pulse. This is called "pulse compression".

2.2. Pulse Compression

The term radar signal processing incorporates the choice of transmitting waveforms for various radars, detection theory, performance evaluation, and the circuitry between the antenna and the displays or data processing computers. The relationship of signal processing to radar design is analogous to modulation theory in communication systems. Both fields continually emphasize communicating a maximum of information in a special bandwidth and minimizing the effects of interference.

Although the transmitted peak power was already in megawatts, the peak power continued to increase more and more due to the need of longer range detection. Besides the technical limitation associated with it, this power increase poses a financial burden. Not only that, target resolution and accuracy became unacceptable. Siebert [2.3] and others pointed out the detection range for a given radar and target was dependent only on the ratio of the received signal energy to noise power spectral density and was independent of the waveform. The efforts at most radar laboratories then switched from attempts to construct higher power transmitters to attempts to use pulses that were of longer duration than the range resolution and accuracy requirements would allow.

Increasing the duration of the transmitted waveform results in increase of the average transmitted power and shortening the pulse width results in greater range resolution. Pulse compression is a method that combines the best of both techniques by transmitting a long coded pulse and processing the received echo to get a shorter pulse.

The transmitted pulse is modulated by using frequency modulation or phase coding in order to get large time-bandwidth product. Phase modulation is the widely used technique in radar systems. In this technique, a form of phase modulation is superimposed to the long pulse increasing its bandwidth. This modulation allows discriminating between two pulses even if they are partially overlapped. Then upon receiving an echo, the received signal is compressed through a filter and the output signal will look like the one. It consists of a peak component and some side lobes.

2.2.1. Phase coded pulse compression

In this form of pulse compression, a long pulse of duration T is divided into N sub-pulses each of width τ as shown in Figure 2.2. An increase in bandwidth is achieved by changing the phase of each sub-pulse. The phase of each sub-pulse is chosen to be either 0 or π radians. The output of the matched filter will be a spike of width τ with an amplitude N times greater than that of long pulse. The pulse compression ratio is $N = T/\tau \approx BT$, where $B \approx 1/\tau$ = bandwidth. The output waveform extends a distance T to either side of the peak response, or central spike. The portions of the output waveform other than the spike are called time side-lobes.

2.2.2. Barker codes

The binary choice of 0 or π phase for each sub-pulse may be made at random. However, some random selections may be better suited than others for radar application. One criterion for the selection of a good "random" phase-coded waveform is that its autocorrelation function should have equal time side-lobes [2.1]. The binary phase-coded sequence of 0, π values that result in equal side-lobes after passes through the matched filter is called a Barker code. An example is shown in Figure 2(a). This is a Barker code of length 13. The (+) indicates 0 phase and (−) indicates π radians phase. The auto-correlation function, or output of the matched filter, is shown in Figure 2(b). There are six equal time side-lobes to either side of the peak, each of label 22.3 dB below the peak. The longest Barker code length is 13. The barker codes are listed in Table 2.1. When a larger pulse-compression ratio is desired, some form of pseudo random code is usually used. To achieve high range resolution with-out an incredibly high peak power, one needs pulse compression.

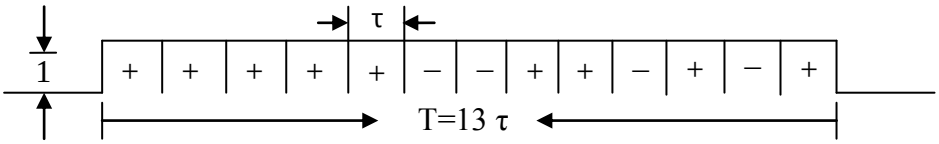

(a) 13-element Barker Code

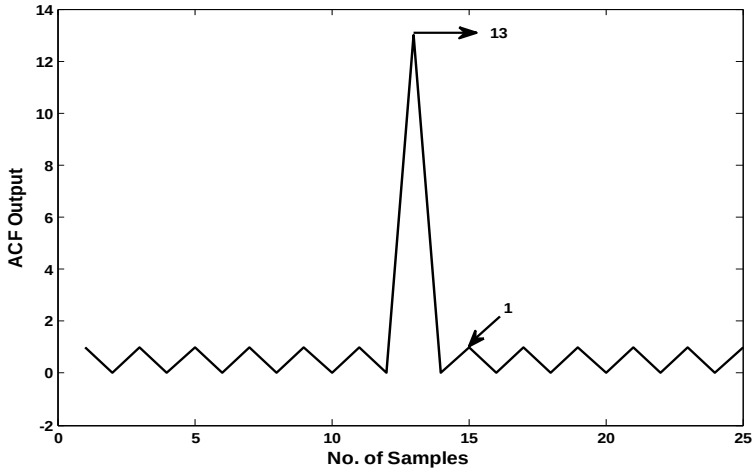

(b) Autocorrelation Output

Figure 2.2. Pulse compressed signal

Table 2.1 Barker codes

Code Length	Code Elements	Sidelobe level, dB
2	+ −, + +	−6.0
3	+ + −	−9.5
4	+ + − +, + + + −	−12.0
5	+ + + − +	−14.0
7	+ + + − − + −	−16.9
11	+ + + − − − + − − + −	−20.8
13	+ + + + + − − + + − + − +	−22.3

2.3. Matched filter

A matched filter is a linear network that maximises the output peak-signal to noise (power) ratio of a radar receiver which in turn maximizes the detectability of a target. It has a frequency response function which is proportional to the complex conjugate of the signal spectrum.

$$H(f) = G_a S^*(f) \exp(-j2\pi f t_m) \quad (2.2)$$

where G_a is a constant, t_m is the time at which the output of the matched filter is a maximum (generally equal to the duration of the signal), and $S^*(f)$ is the complex conjugate of the spectrum of the (received) input signal s(t), found from the Fourier transform of the received signal s(t) such that

$$S(f) = \int_{-\infty}^{\infty} s(t) \exp(-j2\pi ft)\, dt \tag{2.3}$$

A matched filter for a transmitting a rectangular shaped pulse is usually characterized by a bandwidth B approximately the reciprocal of the pulse with τ or $B\tau \approx 1$. The output of a matched filter receiver is the cross-correlation between the received waveform and a replica of the transmitted waveform.

Instead of matched filter, an N-tap adaptive filter is used, by taking input as 13-bit barker code [1 1 1 1 1 -1 -1 1 1 -1 1 -1 1] and desired output as [12zeros 1 12zeros], and weights are trained using different adaptive filtering algorithms.

2.4. Adaptive Filtering Techniques

The adaptive filter is a powerful device for signal processing and control applications because of its ability to operate satisfactorily in an unknown environment and track time variations of input statistics. Adaptive filters have been successfully applied in many diverse fields such as radar, sonar, communications, seismology and biomedical engineering [2.7]. The architecture of an adaptive filter which is a linear combiner is depicted in Figure 2.3. The basic feature of any adaptive filter in common is that an input vector X and desired response d are used to compute an estimated error e which in turn controls the values of a set of adjustable filter coefficients. There are many algorithms that are in use for updating of these filter coefficients. The Least Mean Square (LMS) algorithm, Recursive Least Squares (RLS) algorithm and modified RLS algorithms for adaptive linear combiner are described in this thesis and their performances are compared.

2.4.1. LMS Algorithm

The LMS algorithm is very significant algorithm for many adaptive signal processing applications because of its ease of computation and its simplicity and it doesn't require repetitions of data and off-line gradient estimations. Let $X_k = [\, x_k, x_{k-1}, x_{k-2}, \ldots, x_{k-N+2}, x_{k-N+1}]$ is input vector given to combiner in serial form [2.7, 2.8]. $W_k = [w_0, w_1, w_2, \ldots, w_{N-2}, w_{N-1}]$ is weight vector which are tap weights. Now the linear combiner output is given by

$$y_k = X_k^T W_k \tag{2.4}$$

The error signal with time index k is given by

$$\begin{aligned} e_k &= d_k - y_k \\ &= d_k - X_k^T W_k \end{aligned} \tag{2.5}$$

Where d_k is the desired response at time index k.

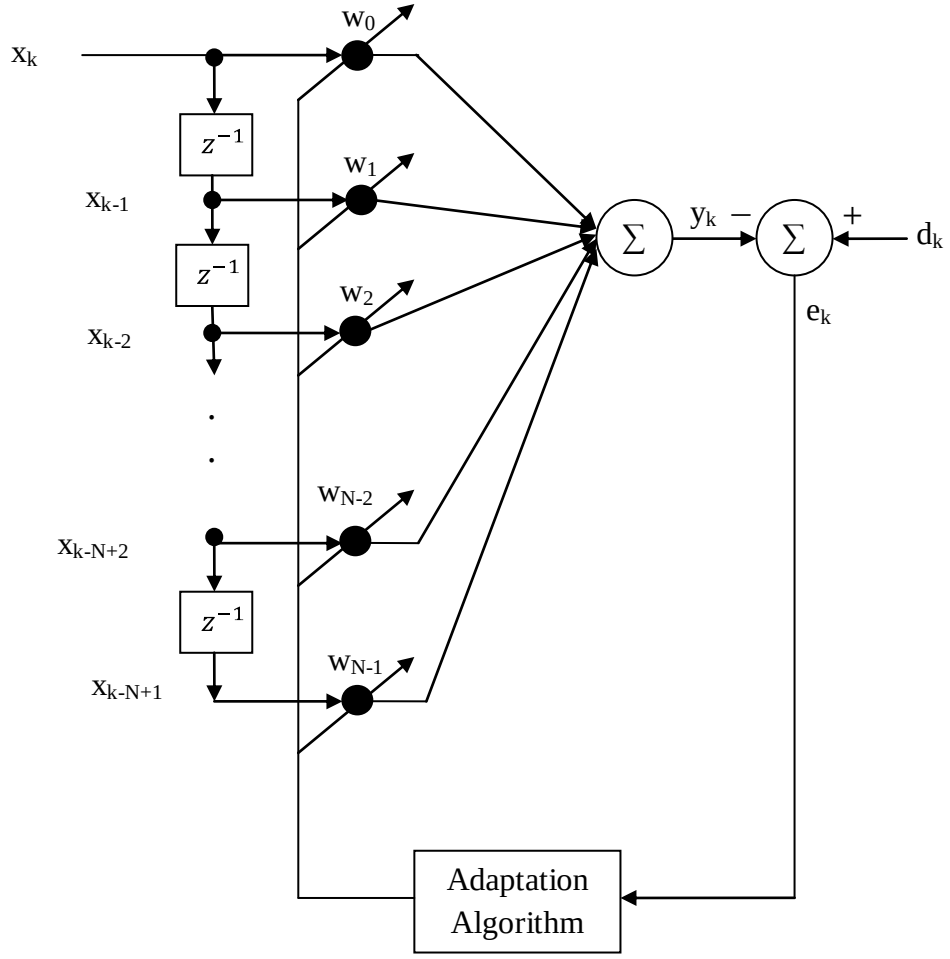

Figure 2.3. The architecture of adaptive linear combiner.

To develop LMS algorithm, e_k^2 is taken as the estimate of gradient. Then in the adaptive process at each iteration, the gradient estimate will be of the form:

$$\hat{\nabla}_k = \begin{bmatrix} \frac{\partial e_k^2}{\partial w_0} \\ . \\ . \\ . \\ \frac{\partial e_k^2}{\partial w_{N-1}} \end{bmatrix} = 2e_n \begin{bmatrix} \frac{\partial e_k}{\partial w_0} \\ . \\ . \\ . \\ \frac{\partial e_k}{\partial w_{N-1}} \end{bmatrix} = -2e_k X_k \qquad (2.6)$$

Where the derivatives of e_k with respect to weights is computed by equation (2.5).

The method of steepest descent type of adaptive algorithm is expressed as

$$W_{k+1} = W_k - \mu \hat{\nabla}_k \qquad (2.7)$$

Substituting (2.6) in (2.7) we get the updation equation of weights in LMS algorithm as follows

$$W_{k+1} = W_k + 2\mu e_k X_k \qquad (2.8)$$

Where μ is the gain constant that regulates the step size. It has the dimensions reciprocal to that of signal power. The weights are updated for each iteration until the estimate of the gradient gets minimised.

2.4.2. RLS Algorithm

RLS algorithm was developed based on matrix inversion lemma. The main advantage of RLS over LMS algorithm is that its convergence rate is faster than that of LMS filters [2.7, 2.8]. But this advancement in performance is attained at the expense of an increase in computational complexity of the RLS filter. To derive the RLS algorithm, let X_k represents the input vector and d_k represents desired response of the RLS filter.

2.4.2.1. Steps in RLS Algorithm

The steps involved for updating optimal weight vector is given in this section. The inverse of autocorrelation function, R_k^{-1} is assumed to exist. The steps then proceed as follows.

- Accept $\{x_k, d_k\}$ as new samples.
- Form X(k) by shifting x(k) into information vector.

- Compute the aprior output

$$y_0(k) = W_k^{0T} X(k) \tag{2.9}$$

- Compute a priori error

$$e_0(k) = d(k) - y_0(k) \tag{2.10}$$

- Compute the filtered information vector

$$Z(k) = R_k^{-1} X(k) \tag{2.11}$$

- Compute the normalised error power

$$q = X^T(k) Z(k) \tag{2.12}$$

- Compute the gain constant

$$\nu = \frac{1}{1+q} \tag{2.13}$$

- Compute normalised information vector

$$\overline{Z}(k) = \nu Z(k) \tag{2.14}$$

- Compute the optimal weight vector W_k^0 to W_{k+1}^0

$$W_{k+1}^0 = W_k^0 + e_0(k).\overline{Z}(k) \tag{2.15}$$

- Update the inverse correlation matrix

$$R_{k+1}^{-1} = R_k^{-1} - \overline{Z}(k).\overline{Z}^T(k) \tag{2.16}$$

R_k^{-1} is initialised as follows

$$R_k^{-1} = \eta I_N \tag{2.17}$$

Where I_N is an identity matrix of order NxN. η value is initialised as a large number of about 10^3 or 10^4.

2.4.3. Modified RLS Algorithm

A modification of standard RLS algorithm has been performed by introducing a criterion:

$$\left|e_k\right| \geq TH \tag{2.18}$$

Where TH represents a threshold value to which the instantaneous error value is being compared. If the instantaneous error value is greater than or equal to the threshold value, then

the updation of estimated filter coefficients vector W_k is performed. Otherwise the correction of weight vector is not performed [2.10].

The threshold value is initialised to a less value and later it is updated for each iteration based on the maximum error value at that iteration. The updation for threshold value at jth iteration is given by

$$MAX\_ERR_j = \max(e_k) \tag{2.19}$$

$$TH_j = \delta.MAX\_ERR_j \tag{2.20}$$

Where e_k is the error vector at jth iteration. MAX_ERR_j is the maximum value of all the errors in error vector. δ is the constant whose value is close or equal to 1 and it affects the rate of convergence.

Hence the estimated weight vector updation is performed only at the time instants when the instantaneous error exceeds or comes close to maximum error value from last iteration step. The modified RLS algorithm attempts to minimise the maximum error value at the filter output.

2.5. Simulation Results and Discussion

The 13-tap adaptive filter is taken and the weights are trained by using LMS, RLS and modified RLS algorithms. The 13-bit barker code is given as the input to the filter. The desired output must be only main lobe and all sidelobes should be zeros. So desired output will be [12zeros 1 12zeros] for 13-bit barker code. The filter should be trained such a way that all sidelobes should be minimized and only main lobe should be present. The signal-to-sidelobe ratio (SSR) performance and noise performances are compared for LMS, RLS, modified RLS algorithms.

2.5.1. SSR Performance:

Signal-to-sidelobe ratio is an important parameter in pulse compression. SSR is the ratio of peak signal amplitude to maximum sidelobe amplitude.

$$SSR_{[dB]} = 20\log_{10}\frac{P_{signal}}{P_{sidelobe}} \tag{2.21}$$

The SSR is calculated when 13-bit barker code is given as input to filter and the values are compared for matched filter (ACF), LMS, RLS, modified RLS and are depicted in table 2.2. The SSR value is large for modified RLS and its value is 25.74dB. The compressed waveforms using ACF, LMS, RLS and modified RLS algorithms are shown in Figure 2.4.

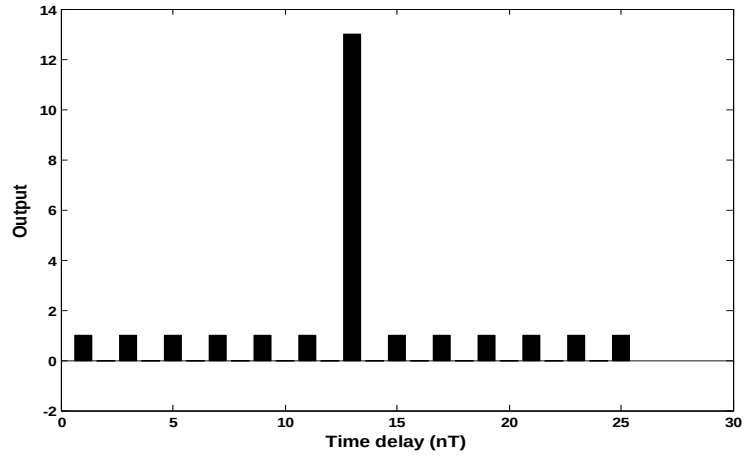

(a)

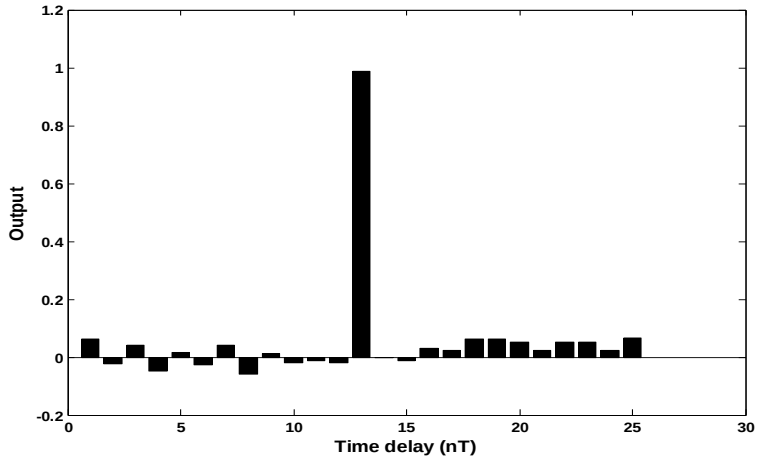

(b)

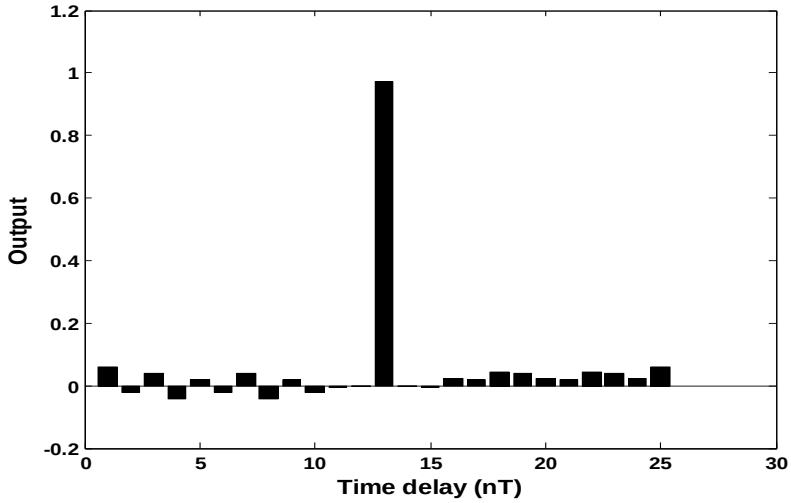

(c)

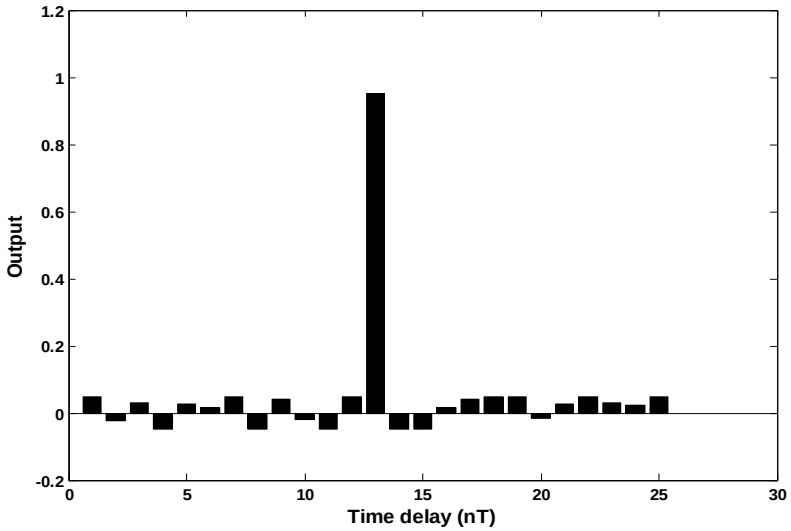

(d)

Figure 2.4. Compressed waveforms for 13-bit barker code using (a) ACF (b) LMS (c) RLS (d) Modified RLS algorithms.

2.5.2. Noise Performance:

The additive white Gaussian noise is added to input signal code then the output is degraded and SSR is decreased gradually. The noise performance at different SNRs using 13-bit barker codes for ACF, LMS, RLS and modified RLS are shown in Figure 2.5 and SSR at different SNRs are listed in Table 2.2.

Table 2.2. SSR performance and SSR comparison for different SNRs for 13-bit barker code

Algorithms	SSR in dB	SSR in dB for different SNRs					
		SNR=1dB	5 dB	10 dB	15 dB	20 dB	25 dB
ACF	22.27	2.98	8.39	13.08	16.38	18.61	20.08
LMS	23.56	2.55	9.03	15.05	19.89	22.70	23.39
RLS	24.00	4.20	10.47	16.32	20.95	23.89	23.94
Modified RLS	25.74	4.01	10.31	16.23	20.98	23.99	24.74

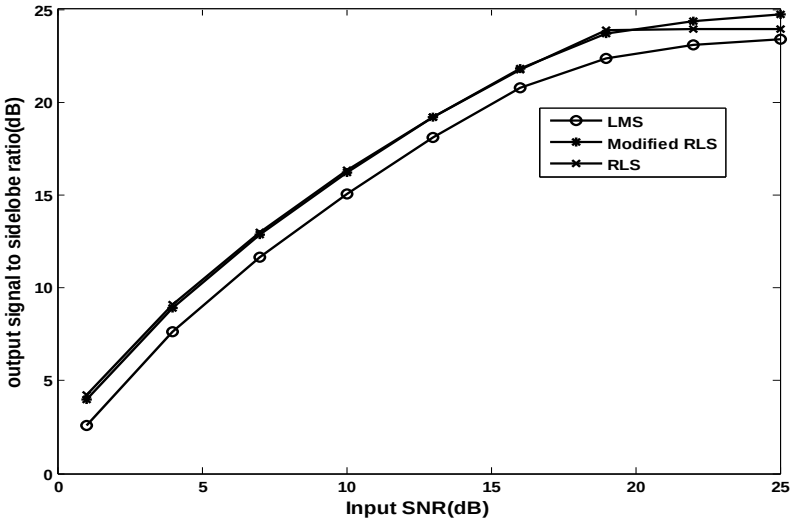

Figure 2.5. Noise performance at different SSRs for 13-bit barker code for LMS, RLS, Modified RLS algorithms

2.6. Summary

In this section the concept of pulse compression in radar is discussed. The concept of phase coded pulse compression and different barker codes are studied. The Adaptive filtering techniques such as LMS, RLS, and modified RLS algorithms are described in detail and their application to pulse compression are discussed. The simulation results using all these three algorithms are discussed and they are compared.

Chapter – 3

A Recurrent Neural Network Approach to Pulse Radar Detection

3.1. Introduction

In radar, high range resolution and range accuracy is obtained by short duration pulses. If the radar is operating with sufficiently narrow pulse widths, then it has the ability to perform limited target classification. But to achieve long ranges with short pulses, a high peak power is required for large pulse energy [3.1]. Also, a reduction in pulse widths reduces the maximum range of radar. Pulse compression allows radar to achieve the energy of a long pulse and resolution of a short pulse simultaneously, without high peak power required of a high energy short-duration pulses. In pulse compression technique a long coded pulse is transmitted and the received echo is processed to obtain a relatively narrow pulse. Thus increased detection capability of a long pulse radar system is achieved while retaining the range resolution capability of a narrow pulse system. The range resolution is determined by bandwidth of the signal. Wide bandwidth is necessary for good range resolution. The signal bandwidth is obtained by modulating phase or frequency of the signal, while maintaining constant pulse amplitude. Mostly biphase pulse compression is used in radar system in which the phase of the transmitted signal is 0 degree relative to a local reference for a '+1' in the binary code and 180 degree for a '-1'.There are two different approaches for pulse compression. The first one is to use a matched filter where codes with small side lobes in their ACF are used. In second approach, two kinds of inverse filters, namely, recursive time variant and non recursive time invariant causal filter are used.

The importance of the detection filter design is to reduce the output range sidelobe level to an acceptable level. To suppress the sidelobes of Barker code of length 13, an adaptive finite impulse response(FIR) filter is placed next to a matched filter pulse[3] and the filter is implemented via two approaches: least mean square (LMS) and recursive least square (RLS) algorithms [3.4]. Zrnik *et. al* [3.5] proposed a self -clutter suppression filter design using the modified recursive least square (RLS) algorithm which gives better performance compared to iterative RLS and ACF algorithms. A multilayered neural network approach which yields better SSR than basic autocorrelation approach is reported in [3.6]. There is a scope of further improvement in performance in terms of SSR, error convergence speed, and doppler shift. In this chapter, a new approach using Recurrent Neural Network (RNN) is proposed, and the results are compared with neural networks and other algorithms like ACF. The concept of neural networks, Multilayer perceptron and recurrent neural networks are described and their simulation results are compared.

3.2. Artificial Neural Network

In recent years, the Artificial neural network (ANN) has become as a powerful learning tool to perform complex tasks in non-linear signal processing environment because of its good learning capability and massively parallel distributed structure. These are extensively used in the field of communication, control, instrumentation and forecasting. The ANN commonly called as 'neural networks' takes its name from the network of nerve cells in the brain. ANN was found to be an important technique for many classification and optimization problems. McCulloch and Pitts have developed the neural networks for different computing machines [3.7]. The ANN is capable of performing nonlinear mapping between the input and output space due to its massive parallel interconnection between different layers and the nonlinear processing characteristics.

An artificial neuron basically consists of a computing element that performs the weighted sum of the input signal and the connecting weight. The sum is added with the bias or threshold and the resultant signal is then passed through activation function like sigmoid or hyperbolic tangent type which is non-linear in nature. Each neuron consists of three parameters namely, the connecting weights, the bias and the slope of the nonlinear function whose learning can be adjusted. From the structural point of view, a NN may be single layer or multilayer. In multilayer structure, there is more than one layer, and in each layer there are more than one artificial neuron. Each neuron of the one layer is connected to each and every neuron of the following layer. The two types of NNs namely Multi Layer Perceptron (MLP), and Recurrent Neural Network (RNN) are discussed in the thesis and the results are compared.

3.2.1. Single Neuron Structure

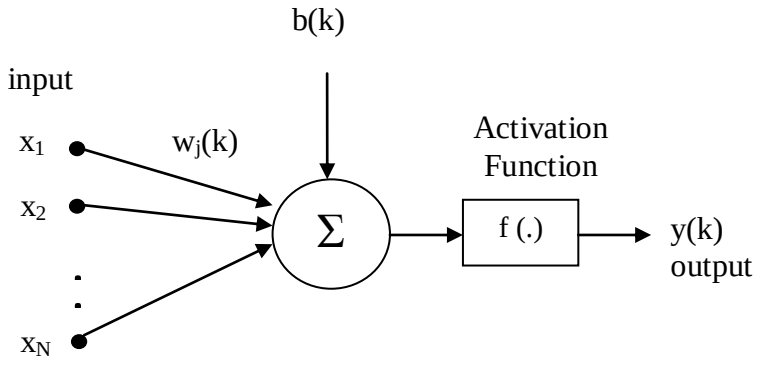

Figure 3.1. Structure of single neuron

The structure of a single neuron is shown in figure 3.1. The output associated with the neuron is computed as,

$$y(k) = f\left[\sum_{j=1}^{N} w_j(k)x_j(k) + b(k)\right] \tag{3.1}$$

Where x_1, x_2,.., x_N are inputs to neuron, w_j is the synaptic weights of the jth input, b_k is the bias or threshold, N is the total number of inputs given to the neuron and f(.) is the nonlinear activation function. Some non-linear activation functions are discussed here.

Log-Sigmoid function:

This transfer function takes the input and squashes the output into the range of 0 to 1, according to expression given below [3.8].

$$f(x) = \frac{1}{1+e^{-x}} \tag{3.2}$$

This function is most commonly used in multilayered networks that are trained by back propogation algorithm.

Hyperbolic tangent Sigmoid:

This function is represented as

$$f(x) = \tanh(x) = \frac{e^{x} - e^{-x}}{e^{x} + e^{-x}} \tag{3.3}$$

Where x is input to the hyperbolic function

Signum Function:

The expression for this activation function is given by

$$f(x) = \begin{cases} 1\ ,\ if\ \ x > 0 \\ 0\ ,\ if\ \ x = 0 \\ -1\ ,\ if\ \ x < 0 \end{cases} \tag{3.4}$$

Threshold Function:

This function is given by the expression

$$f(x) = \begin{cases} 1\ ,\ \ for\ \ x \geq 0 \\ 0\ ,\ \ for\ \ x = 0 \end{cases} \tag{3.5}$$

Piecewise linear Function:

This function represented as follows

$$f(x)=\begin{cases}1\ ,\ if\ \ x\geq\dfrac{1}{2}\\ x\ ,\ if\ \ -\dfrac{1}{2}>x>\dfrac{1}{2}\\ 0\ ,\ if\ \ x\leq 0\end{cases} \tag{3.6}$$

where the amplification factor inside the linear region of operation is assumed to be unity.

3.2.2. Multilayer Perceptron

In the multilayer perceptron, the input signal propagates through the network in the forward direction, on a layer by layer basis. This network has been applied successfully to solve some difficult and diverse problems by training in a supervised manner with a highly popular algorithm known as the error back-propagation algorithm. The structure of MLP for three layers is shown in Figure 3.2.

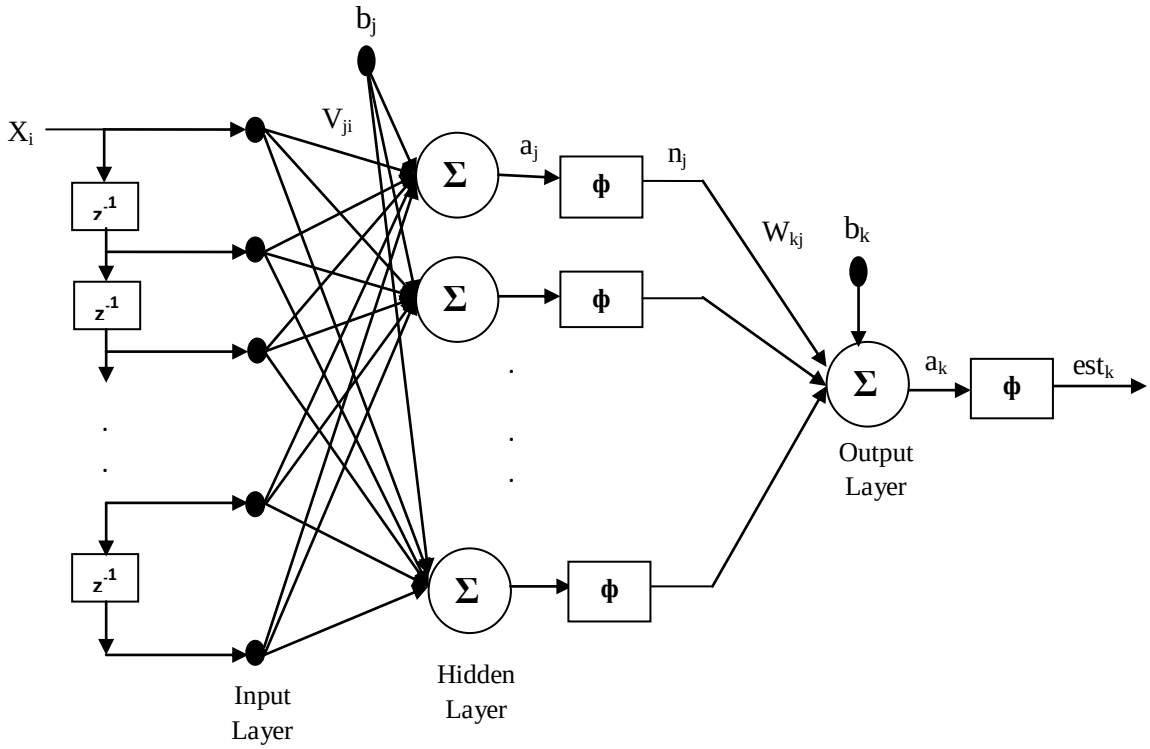

Figure 3.2. Structure of MLP

The Three layers are input, hidden and output layers. Let each layer has its own index variable, 'k' for output nodes, 'j' for hidden nodes and 'i' for input nodes. The input vector is propagated through a weight layer **V**. The output of jth hidden node is given by,

$$n_j(t) = \varphi(a_j(t)) \tag{3.7}$$

$$\text{where} \quad a_j(t) = \sum_i x_i(t)\, v_{ji} + b_j \tag{3.8}$$

and a_j is output of jth hidden node before activation. x_i is the input value at ith node. b_j is the bias for jth hidden node, and φ is the activation function. The logistic function is used as activation function for both hidden and output neurons and is represented by,

$$\varphi(y) = \frac{1}{1+e^{-y}} \tag{3.9}$$

The output of the MLP network is determined by a set of output weights, **W**, and is computed as,

$$est_k(t) = \varphi(a_k(t)) \tag{3.10}$$

$$a_k(t) = \sum_j n_j(t) w_{kj} + b_k \tag{3.11}$$

Where est_k is the final estimated output of kth output node. The cost function for nth epoch is given by,

$$\xi(n) = \frac{1}{2}\sum_q^N \sum_k (d_{qk} - \text{est}_{qk})^2 \tag{3.12}$$

Where N is the total number of training patterns and q represents pattern given to the network.

The learning algorithm used in training the weights is backpropagation [3.7]. In this algorithm, the correction to the synaptic weight is proportional to the negative gradient of the cost function with respect to that synaptic weight and is given as,

$$\mathbf{\Delta W} = -\eta \frac{\partial \xi}{\partial \mathbf{W}} \tag{3.13}$$

Where η is the learning rate parameter of the back propagation algorithm.

The local gradient for output neurons is obtained to be,

$$\delta_{qk} = -\frac{\partial \xi}{\partial \mathrm{est_{qk}}} \frac{\partial \mathrm{est_{qk}}}{\partial \mathrm{a_{qk}}}$$

$$= \left(d_{qk} - \mathrm{est_{qk}}\right) \varphi'\left(\mathrm{est_{qk}}\right) \tag{3.14}$$

and for hidden neurons,

$$\delta_{qj} = -\left(\sum_{k} \frac{\partial \xi}{\partial \mathrm{est_{qk}}} \frac{\partial \mathrm{est_{qk}}}{\partial \mathrm{a_{qk}}} \frac{\partial \mathrm{a_{qk}}}{\partial \mathrm{n_{qj}}}\right) \frac{\partial \mathrm{n_{qj}}}{\partial \mathrm{a_{qk}}}$$

$$= \sum_{\mathrm{k}} \delta_{qk} w_{kj} \varphi'\left(\mathrm{n_{qj}}\right) \tag{3.15}$$

The correction to output weights is given by,

$$\Delta w_{kj} = \eta \sum_{q}^{N} \delta_{qk}\, \mathrm{n_{qj}} \tag{3.16}$$

And for hidden layer weights,

$$\Delta \mathrm{v}_{ji} = \eta \sum_{q}^{N} \delta_{qj}\, \mathrm{x_{qi}} \tag{3.17}$$

Hence all weights are updated based on the corresponding weight correction equations.

3.2.3. Recurrent Neural Network

The recurrent neural network is a network with feedback connections and has an inherent memory for dynamics that makes them suitable for dynamic system modelling. These networks are computationally more efficient and stable than traditional feed forward networks. Toha and Tokhi [3.13] have used Elman RNN for modeling the twin rotor multi input multi output system. RNN is used for Arabic speech recognition instead of traditional hidden Markov models as described in [3.12].

The simple recurrent network used here is Elman's network as shown in Figure 3.3. This two-layer network has recurrent connections from the hidden neurons to a layer of context units consisting of unit delays [3.13]. These context units store the outputs of hidden neurons for one time step and feed them back to the input layer.

The inputs to the hidden layers are combination of the present inputs and the outputs of the hidden layer which are stored from previous time step in context layer. The outputs of

the Elman network are functions of present state, previous state (that is stored in context units) and present inputs.

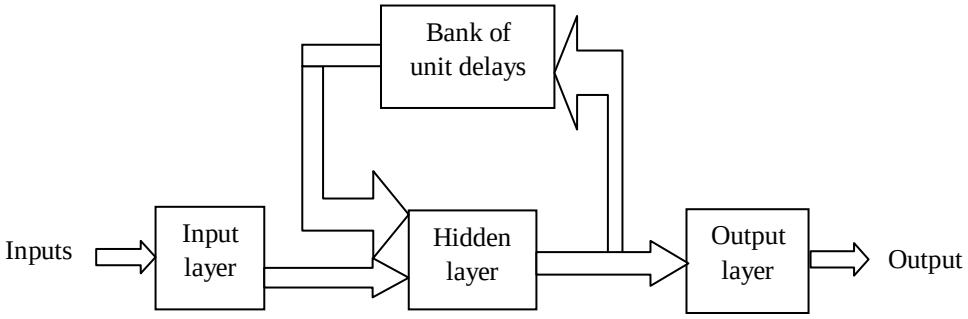

Figure 3.3. Elman's network

Let 'h' represents the index for hidden nodes for recurrent connections. The input vector is propagated through a weight layer **V** and combined with the previous state activation through an additional recurrent weight layer, **U** [3.11]. The output of jth hidden node is given by,

$$n_j(t) = \varphi(a_j(t)) \tag{3.18}$$

$$\text{where} \quad a_j(t) = \sum_i x_i(t)\, v_{ji} + \sum_h n_h(t-1)\, u_{jh} + b_j \tag{3.19}$$

and a_j is output of jth hidden node before activation. x_i is the input value at ith node. b_j is the bias for jth hidden node, and φ is the activation function.

This hidden node is used to compute the final output of Elman's network similarly as in the case of equation (3.10). The local gradients for output neurons and hidden neurons are obtained in similar way as in equations (3.14), (3.15). The correction to output weights and hidden layer weights are also computed using (3.16), (3.17).
The correction to recurrent weights is given by,

$$\Delta u_{kj} = \eta \sum_q^N \delta_{qj}(t)\, n_{qh}(t-1) \tag{12}$$

Hence all weights are updated based on the corresponding weight correction equations.

3.3. Simulation Results and Discussion

The input signal codes used are 13-bit barker code having the sequence (1,1,1,1,1,-1,-1,1,1,-1,1,-1,1) and 35-bit barker code, which are phase modulated waveforms. The 35-bit code is obtained by Kronecker tensor product of 5-bit and 7-bit barker codes. These input codes are time shifted and given as training samples for the network to be trained. The target or desired signal code whose length is equal to length of autocorrelation function of input, is '1', when training set at the network is input code, and for the other sets it is '0'. Both the MLP and RNN networks are trained by using back propagation algorithm which is discussed in previous section.

The training is performed for 1000 iterations. The weights of all the layers are initialized to random values between ±0.1 and the value of η is taken as 0.99. After the training is completed, the networks are employed for radar pulse detection. In this section, the performances of RNN, MLP and ACF are compared by taking 13-bit and 35-bit barker codes. The convergence performance, SSR performance, noise performance, range resolution ability, and Doppler shift performance are obtained.

3.3.1. Convergence Performance

The mean square error curves of recurrent neural network and MLP for 13-bit and 35-bit barker codes are shown in Figure 3.4.

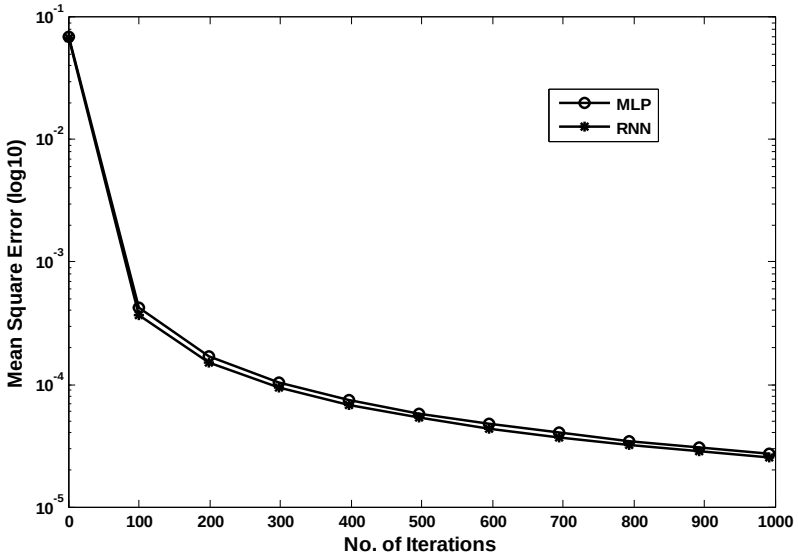

(a)

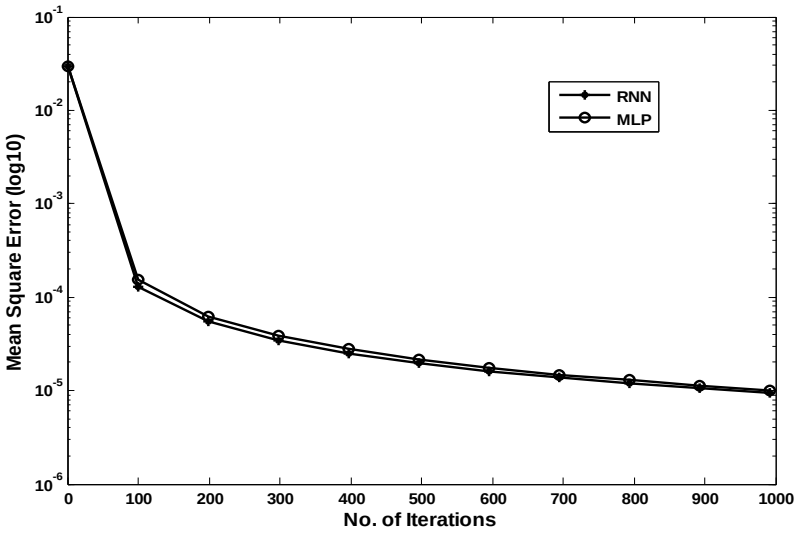

(b)

Figure 3.4. Mean Square Error Curve of RNN and MLP for (a) 13-bit and (b) 35-bit barker code

It is observed from the figure that, the RNN provides better convergence speed than that of MLP.

3.3.2. SSR Performance

Signal-to-sidelobe ratio is the ratio of peak signal amplitude to maximum sidelobe amplitude [3.6]. The SSR in this case is calculated using RNN based approach.

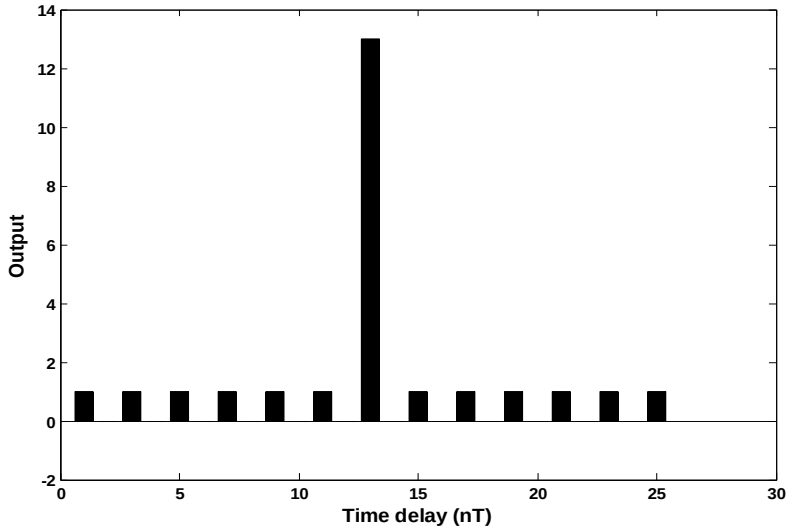

(a)

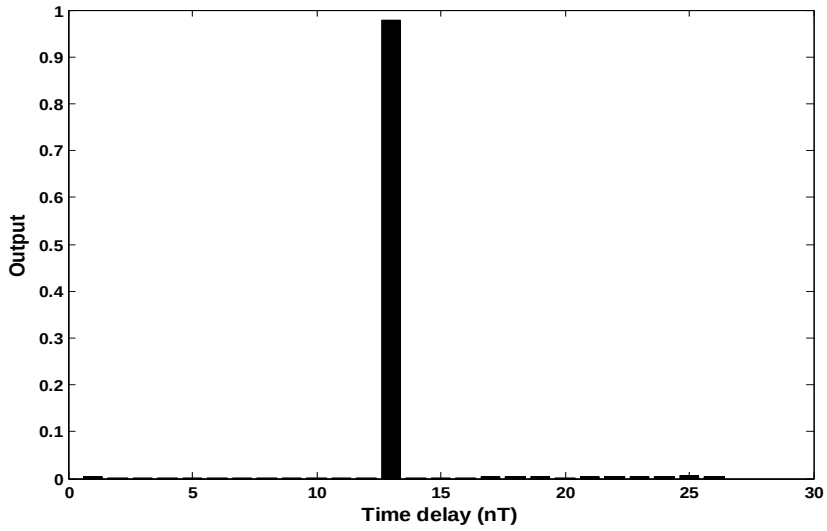

(b)

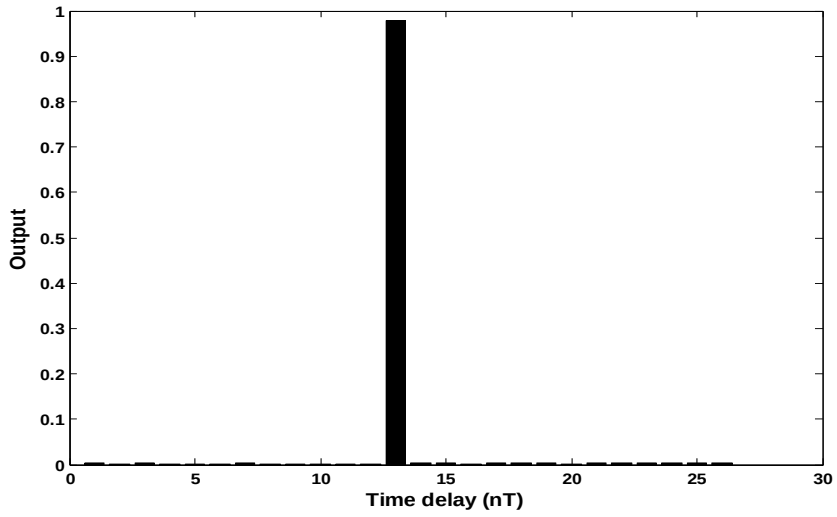

(c)

Figure. 3.5. Compressed waveforms for (a) ACF (b) MLP (c) RNN for 13-bit barker code

It is compared with those obtained by MLP and ACF algorithms for 13-bit and 35-bit barker codes. The results are tabulated in Table 3.1, which shows that RNN gives improved SSR than other algorithms. The compressed waveforms for 13-bit barker code are shown in Figure 3.5.

Table 3.1. SSR comparison in dB

Algorithms	13-Bit Barker Code	35-Bit Barker Code
ACF	22.27	13.97
MLP	45.13	44.41
RNN	47.91	47.72

3.3.3. Noise Performance

The additive white Gaussian noise is added to input signal code then the output is degraded and SSR is decreased gradually. The noise performance at different SNRs using 13-bit and 35-bit barker codes for RNN and MLP are shown in Figure 3.6 and SSR at different SNRs are listed in Table 3.2 and 3.3. The results show that RNN achieved higher SSR compared to all other approaches.

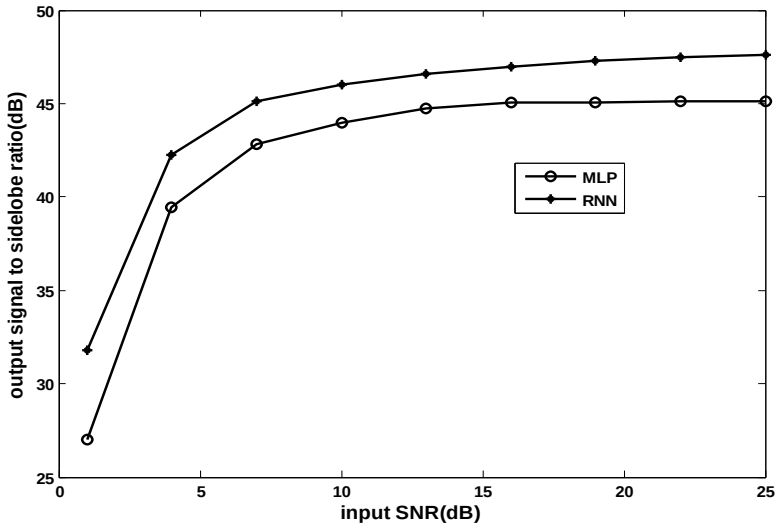

(a)

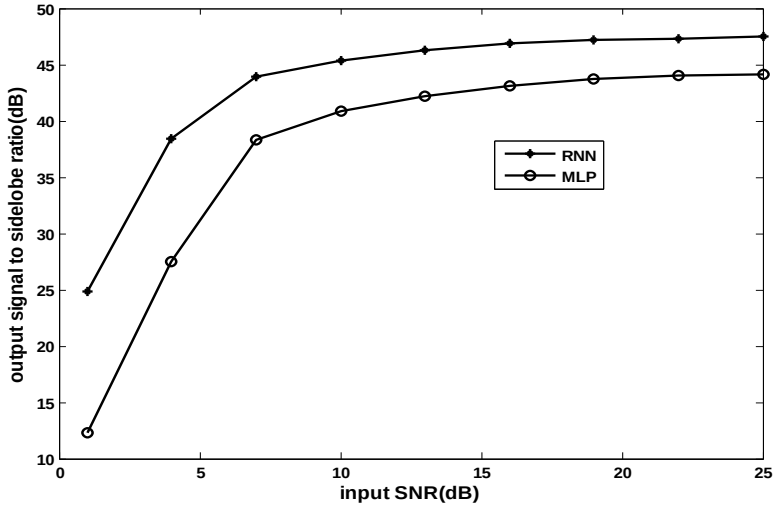

(b)

Figure 3.6. Noise performances for different SNRs using (a) 13-bit and (b) 35-bit barker codes

Table 3.2. SSR Comparison for Different SNRs for 13-Bit Barker Code

Algorithms	SNR= 1dB	5dB	10dB	15dB	20dB	25dB
ACF	2.98	8.39	13.08	16.38	18.61	20.08
MLP	27.00	41.67	43.97	45.05	45.08	45.10
RNN	31.78	44.30	46.01	46.88	47.34	47.59

Table 3.3. SSR Comparison for Different SNRs for 35-Bit Barker Code

Algorithms	SNR= 1dB	5dB	10dB	15dB	20dB	25dB
ACF	9.26	10.86	12.09	12.87	13.34	13.61
MLP	12.34	31.62	40.84	42.84	43.87	44.11
RNN	24.85	41.14	45.35	46.73	47.24	47.45

3.3.4. Range Resolution Ability

Range resolution is the ability of radar to resolve two or more targets at different ranges. If two targets are considered, they should be separated by minimum range equal to the width of processed echo pulse. The two waveforms are overlapped by delaying the second one by some delays and are applied as input to the network and SSR is calculated. The performance of RNN is observed to be better than others and is depicted in Table 3.4, varying the delays from 2 to 5. Figure 3.7 shows the compressed waveforms of the added pulse trains with five-delay-apart having same magnitude for 13-bit barker code.

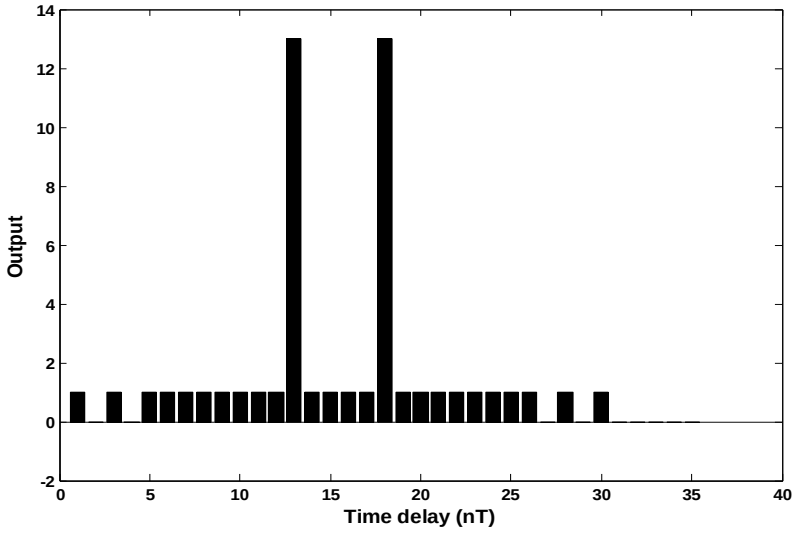

(a)

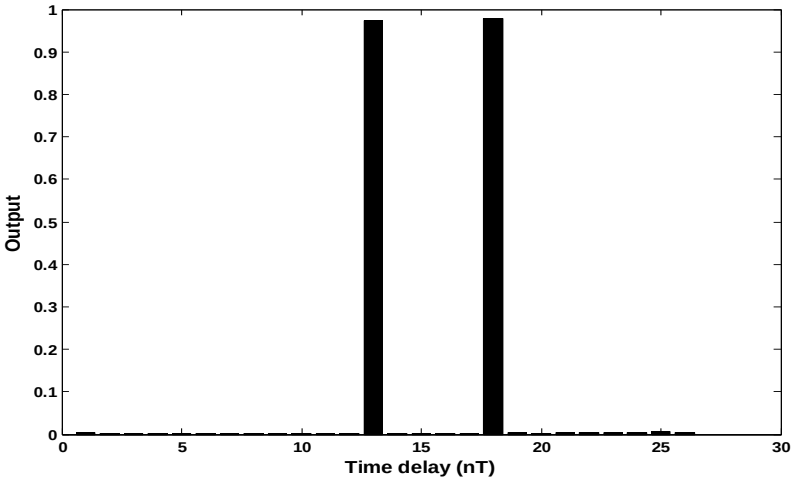

(b)

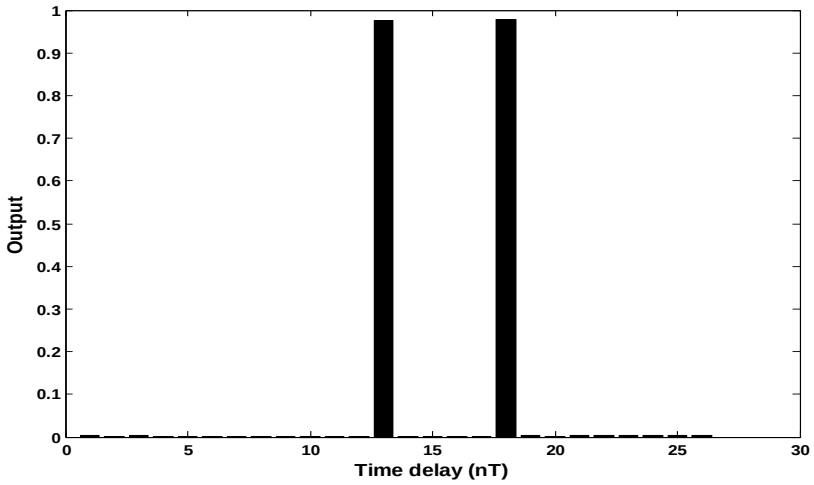

(c)

Figure 3.7. Compressed waveforms for 13-bit barker code having same IMR and 5 DA (a) ACF (b) MLP (c) RNN

By varying the magnitude of one input or changing the input magnitude ratio (IMR), which is the ratio of magnitude of the first pulse train to the delayed one, the SSR values are calculated and listed in Table 3.5.

Table 3.4. SSR Comparison in dB for Range Resolution Ability of Two Targets Having Same IMR but Different Delays for 13-Bit Barker Code

Algorithms	2-DA	3-DA	4-DA	5-DA
ACF	16.90	22.3	16.90	22.3
MLP	45.09	45.1	45.10	45.08
RNN	47.89	47.88	47.89	47.87

Table 3.5. SSR Comparison in dB for Range Resolution Ability of Two Targets Having Different IMRs and Different Delays for 13-Bit Barker Code

Algorithms	2-DA 2-IMR	3-DA 3-IMR	4-DA 4-IMR	5-DA 5-IMR
ACF	13.97	12.74	10.63	8.29
MLP	44.97	44.44	36.18	11.00
RNN	45.45	47.57	42.15	22.16

3.3.5. Doppler Tolerance

The Doppler sensitivity is caused by shifting the phase of individual elements of the phase code. In the extreme case, the codeword is no longer matched with the replica, if the last element is shifted by 180º. For 13-bit barker code, the code is changed from (1,1,1,1,1,-1,-1,1,1,-1,1,-1,1) to (-1,1,1,1,1,1,-1,-1,1,1,-1,1,-1,1) and is fed to the network. The SSR is then calculated for both 13-bit and 35-bit barker codes and depicted in Table 3.6. The compressed waveforms under Doppler shift conditions for ACF, MLP and RNN are shown in Figure 3.8. The results show that RNN gives better SSR compared to other networks.

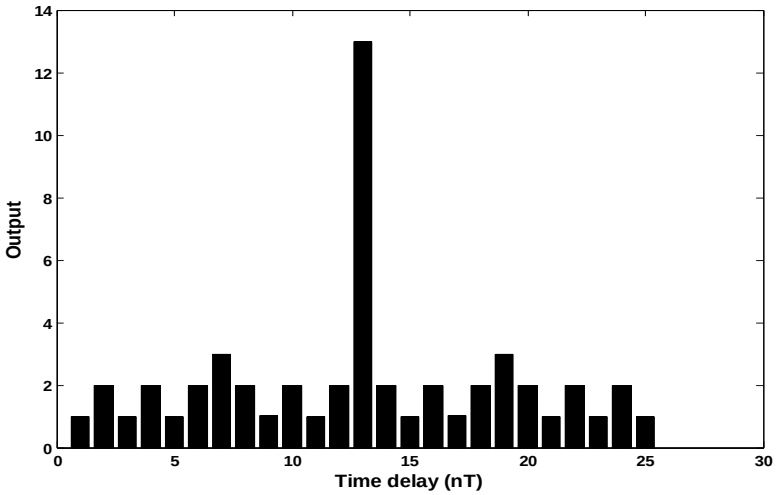

(a)

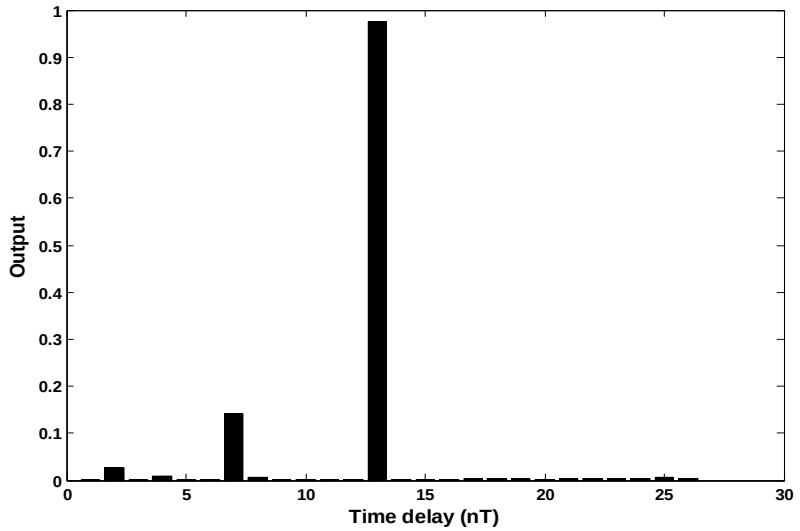

(b)

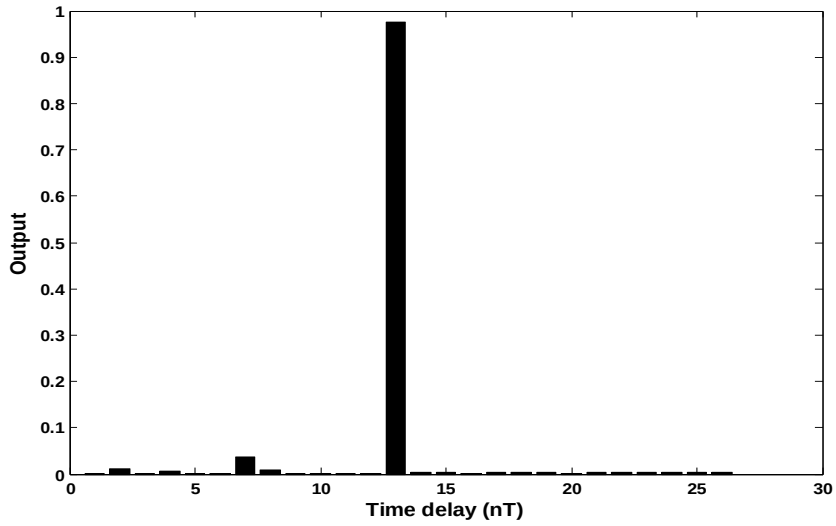

(c)

Figure 3.8. Compressed waveforms for Doppler tolerance for 13-bit barker code (a) ACF (b) MLP (c) RNN

Table 3.6. Doppler shift performance in dB

Algorithms	13-bit barker code	35-bit barker code
ACF	12.74	13.97
MLP	16.38	44.34
RNN	27.68	47.71

3.4. Summary

In this chapter, the concepts of artificial neural network, multilayer perceptron and recurrent neural network are studied. Elman's recurrent neural network is applied for achieving improved pulse compression. The simulation results clearly demonstrate that the RNN gives improved performance than other networks like the MLP and ACF. The RNN gives better error convergence performance compared to that of MLP. From the simulations it is shown that RNN gives significant improvement in noise performance and range resolution ability. Finally under doppler shift conditions, the RNN gives much better SSR of 27.68dB compared to the MLP which is only 16.38dB for 13-bit barker code.

Chapter – 4

A Recurrent RBF Approach to Pulse Radar Detection

4.1. Introduction

Pulse compression plays a significant role in radar systems in achieving good signal strength and high resolution. The good signal strength is achieved by long duration pulses, which reduces the peak power. Transmitting longer pulse increases the sensitivity of radar system by increasing the average transmitted power. But the longer pulse deteriorates the range resolution of the radar [4.7]. For limited target classification, range resolution should be high enough which is obtained by narrow pulses. Hence as a compromise, pulse compression technique is employed in which a long duration pulse is either frequency or phase modulated to increase the bandwidth. This long duration modulated pulse is compressed at the receiver using matched filter [4.1]. In pulse compression technique a long coded pulse is transmitted and the received echo is processed to obtain a relatively narrow pulse. The signal to sidelobe ratio performance, noise performance and Doppler tolerance performance must be considered as major aspects for a pulse compression technique. Based on these considerations many pulse compression techniques have been evolved.

In the previous chapters, the adaptive linear combiner trained by LMS, RLS, modified RLS was implemented for pulse compression. Also, RNN trained by back propagation algorithm was proposed and implemented for pulse radar detection and the simulation results are compared with that of MLP and ACF. There is a scope of further improvement in performance in terms of SSR, error convergence speed, and doppler shift. In this chapter, the concept of radial basis neural network (RBF) is discussed and from that a new approach using Recurrent RBF is proposed. Both the networks are applied to the radar pulse detection application and the results are compared with MLP and ACF.

4.2. Radial Basis Function Neural Network (RBF)

The neural networks, in which the hidden units provide a set of functions that constitute an arbitrary basis for input patterns when they are expanded into hidden space which are radial basis functions are called radial basis function neural networks [4.8]. The structure of RBF neural network is given in Figure 4.1. In its basic form, RBFNN consists of 3 layers, an input layer, a hidden layer and an output layer. The input layer consists of the source nodes, which are also called sensory units, that connect the network to its environment. The unique hidden layer in the network, applies a nonlinear transformation from input space to hidden space using radial basis functions. The hidden space is of higher

dimensionality in most of the applications. The response of the network is supplied by the output layer which is linear in nature.

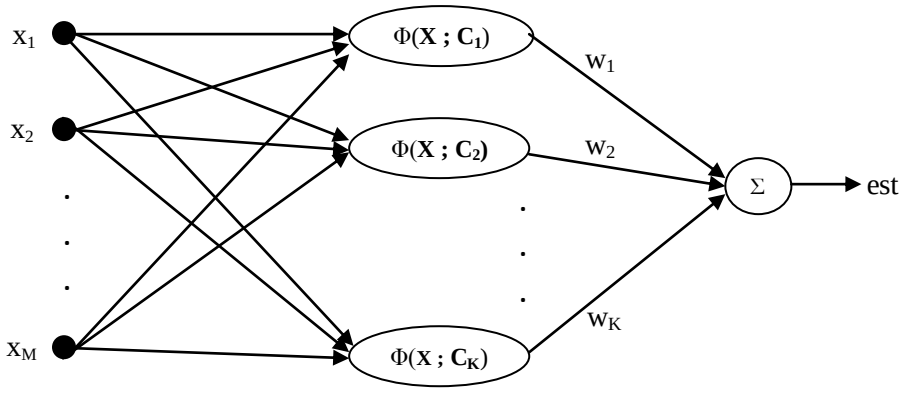

Figure 4.1. Structure of RBF

The output of the network is given by

$$\text{est}_q = \sum_{i=1}^{k} w_i \, . \Phi(\mathbf{X}_q, \mathbf{C}_i) \tag{4.1}$$

Where est is the estimated output of RBF network. Index 'k' represents the number of hidden neurons. w_k represents the weight between kth hidden node and output node. $\mathbf{C}_k$ is the center of kth hidden node. $\Phi(\mathbf{X}_q, \mathbf{C}_k)$ represents the kth radial basis function that computes the Euclidean distance between input vector $\mathbf{X}_q$ and center $\mathbf{C}_k$ at kth node and qth input pattern.

Radial basis functions:

According to Micchelli [4.8], the element of interpolation matrix ϕ which is non singular is given by $\phi(x, c) = \phi(\|x - c\|)$, where $\|.\|$ denotes the Euclidean norm.

1. Multiquadrics:

$$\phi(r) = (r^2 + a^2)^{\frac{1}{2}} \quad for\ a > 0\ and\ r \in \mathbb{R} \tag{4.2}$$

2. Inverse Multiquadrics:

$$\phi(r) = (r^2 + a^2)^{-\frac{1}{2}} \quad for\ a > 0\ and\ r \in \mathbb{R} \tag{4.3}$$

3. Gaussian functions:

$$\phi(r) = \exp\left(-\frac{r^2}{2\sigma^2}\right) for\ \sigma > 0\ and\ r \in \mathbb{R} \tag{4.4}$$

In this thesis, the Gaussian function is used as the radial basis function. Now we get the interpolation matrix ϕ as follows

$$\phi(x,c) = \exp\left(-\frac{\|x-c\|^2}{\sigma^2}\right) \tag{4.5}$$

The output of the kth hidden node by is given by

$$\Phi(\mathbf{X}_q, \mathbf{C}_k) = \exp\left[-\frac{1}{\sigma_k^2} . \left\|\mathbf{X}_q - \mathbf{C}_k\right\|^2\right] \tag{4.6}$$

Where q is the pattern given to the network.

In RBFNN, the three parameters that are to be updated are connecting weights between hidden and output units, w_{qk}, centre C_{qk} and the Gaussian spread σ_{qk}. These are updated by using the supervised learning method, which is similar to LMS algorithm. The cost function that is to be minimised is given by

$$\xi(n) = \frac{1}{2}\sum_q^N e_q^2 \tag{4.7}$$

e_q represents the error signal which is the difference between desired output d and the output obtained by ,

$$\begin{aligned} e_q &= d_q - est_q \\ &= d_q - \left(\sum_{i=1}^{k} w_i \, . \Phi(\mathbf{X}_q, \mathbf{C}_i)\right) \\ &= d_q - \left(\sum_{i=1}^{k} w_i \, . \exp\left[-\frac{1}{\sigma_k^2} . \left\|\mathbf{X}_q - \mathbf{C}_k\right\|^2\right]\right) \end{aligned} \tag{4.8}$$

According to stochastic gradient descent method, in order to minimise cost function, we use the following equations.

$$w_k = w_k + \Delta w_k \tag{4.9}$$

$$C_k = C_k + \Delta C_k \tag{4.10}$$

$$\sigma_k = \sigma_k + \Delta \sigma_k \tag{4.11}$$

The correction to weights between hidden layer and output layer is given by

$$\Delta w_k = \mu \,.\, \sum_q^N e_q . \Phi\left(\mathbf{X}_q, \mathbf{C}_k\right) \tag{4.12}$$

Where μ is the convergence parameter.

The correction to center of kth hidden node is given by

$$\Delta \mathbf{C}_k = \mu \,.\, \sum_q^N \frac{e_q}{\sigma_k^2} \,.\, w_k .\ \Phi\left(\mathbf{X}_q, \mathbf{C}_k\right) . \left(\mathbf{X}_q - \mathbf{C}_k\right) \tag{4.13}$$

The correction to gaussian spread of kth hidden node is given by

$$\Delta \sigma_k = \mu \,.\, \sum_q^N \frac{e_q}{\sigma_k^3} \,.\, w_k .\ \Phi\left(\mathbf{X}_q, \mathbf{C}_k\right) . \left\|\mathbf{X}_q - \mathbf{C}_k\right\|^2 \tag{4.14}$$

Hence all the weights, center and spread are updated according to their corresponding equations.

4.3. Recurrent RBF

The recurrent RBF combined temporal local property of the recurrent neural networks and spatial local property exhibited by standard RBF algorithm. Combination of these two properties has advantages in that the learning process and its convergence is faster while maintaining modelling capability of neural networks.

Bambang developed the RRBF network for adaptive noise cancellation (ANC) systems to compensate non linearity that exist in various loops [4.9]. Ryad and Daniel implemented RRBF network for simple temporal sequence recognition using IBM/ZISC (Zero Instruction Set Computer) [4.10]. This type of network combines features from the spatial representation of time of the Multi Layer Perceptron and the RBF networks. RRBF network used for time series prediction to increase the prediction accuracy is reported in [4.11]. Mimura *et*. al [4.12] designed a RRBF network for digital communication systems in which the channel characteristics are non linear in nature. The RRBF is used to estimate all noise free received signals of nonlinear channel. Hardier proposed a recurrent RBFN for suspension system modeling and wear diagnosis of a damper [4.13]. A dynamic RRBF is applied for color image restoration, which employs a hybrid of two algebraic networks, namely a radial basis function and a MLP network [4.14].The RBFN effectively suppress the noise while preserving the image details.

The proposed RRBF network for pulse radar detection is shown in Figure 4.2. The structure of RRBF is similar to RBF with an input layer, one hidden layer and an output layer. A recurrent connection is added across the hidden neurons on a standard RBF network. The output of each hidden neuron is fed back to the corresponding neuron as input through recurrent weights with unit delay.

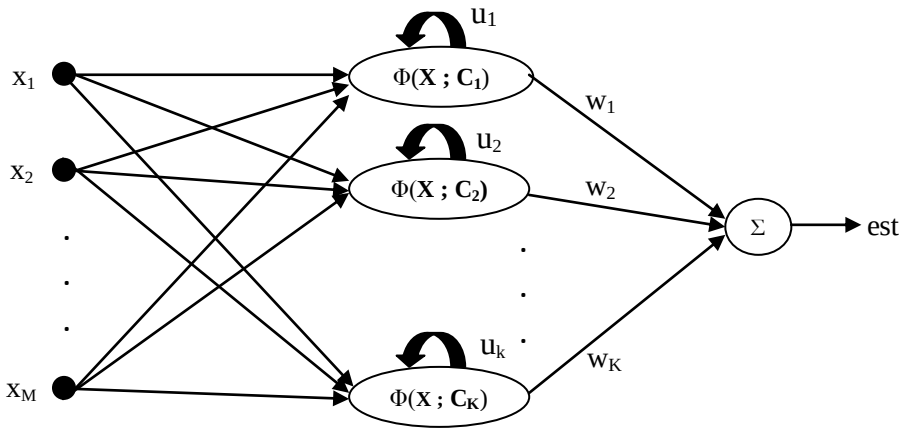

Figure 4.2. Recurrent RBF network

The output of the RRBF network is computed using (4.1). The output of the kth hidden node by considering recurrent weights **U** is computed as

$$\Phi\left(\mathbf{X}_q(n), \mathbf{C}_k(n)\right) = \exp\left[-\frac{1}{\sigma_k^2(n)} . \left\|\mathbf{X}_q(n) - \mathbf{C}_k(n)\right\|^2 + u_{qk} . \Phi\left(\mathbf{X}_q(n-1), \mathbf{C}_k(n-1)\right)\right] \quad (4.15)$$

Where q is the pattern given to the network and n is the present epoch number.

The correction to recurrent weights is obtained as

$$\Delta u_k(n) = \mu . \sum_q^N \frac{\partial \xi(n)}{\partial u_k(n)} \quad (4.16)$$

Where μ is the convergence factor which is close to 1. $\xi(n)$ is the cost function at nth epoch and is given by

$$\xi(n) = \frac{1}{2} \sum_q^N e_q^2(n) \quad (4.17)$$

Where N is the total number of training sets given to the network. e_q is the error for qth training set is

$$e_q(n) = d_q(n) - est_q(n) \tag{4.18}$$

By derivative chain rule,

$$\frac{\partial \xi(n)}{\partial u_k(n)} = \frac{\partial \xi(n)}{\partial est_q(n)} \cdot \frac{\partial est_q(n)}{\partial u_k(n)} = e_q . \frac{\partial est_q(n)}{\partial u_k(n)} \tag{4.19}$$

Where $$\frac{\partial est_q(n)}{\partial u_k(n)} = \frac{\partial est_q(n)}{\partial \Phi(\mathbf{X}_q(n), \mathbf{C}_k(n))} \cdot \frac{\partial \Phi(\mathbf{X}_q(n), \mathbf{C}_k(n))}{\partial u_k(n)}$$

$$= -w_k(n).\ \Phi(\mathbf{X}_q(n), \mathbf{C}_k(n)) .\ \Phi(\mathbf{X}_q(n-1), \mathbf{C}_k(n-1)) \tag{4.20}$$

Substituting (4.20) in (4.19) and finally in (4.16) we get the correction to recurrent weights for kth hidden node as

$$\Delta u_k(n) = -\mu . \sum_q^N e_q . w_k(n).\ \Phi(\mathbf{X}_q(n), \mathbf{C}_k(n)) .\ \Phi(\mathbf{X}_q(n-1), \mathbf{C}_k(n-1)) \tag{4.21}$$

The correction to weights between hidden layer and output layer, center and Gaussian spread are computed in similar way using equations (4.12), (4.13) and (4.14). Hence all the weights, center and spread are updated according to their corresponding equations and the network is trained accordingly.

4.4. Simulation Results and Discussion

The input signal code used is 13-bit barker code having the sequence [1 1 1 1 1 -1 -1 1 1 -1 1 -1 1], which is a phase modulated waveform. This input code is time shifted and given as training samples for the networks to be trained. The target or desired signal code, d, whose length is equal to length of autocorrelation function of input, is '1', when training set at the network is input code, and for the other sets it is '0'.

The training of RRBF is done for both 500 and 1000 epochs. The number of neurons in input layer are taken as 13, in hidden layer are 7 and that of output layer is 1. The convergence factor μ in all updation equations is taken as 0.9. This section discusses about the simulation results obtained by both RBF and RRBF networks and comparison between results of both the networks with RNN, MLP and ACF algorithms by taking 13-bit barker code as input.

4.4.1. Error performance

The error convergence performance for all the neural networks RRBF, RBF, RNN and MLP is clearly illustrated in Fig 2. The mean square error converges to the values, $5.88\text{x}\,10^{-5}$, $5.38\text{x}\,10^{-5}$, $3.11\text{x}\,10^{-6}$ and $1.48\text{x}\,10^{-6}$ for MLP, RNN, RBF and RRBF networks respectively for 500 epochs and converges to values $2.71\text{x}10^{-5}$, $2.52\text{x}10^{-5}$, $8.27\text{x}10^{-7}$ and $6.53\text{x}10^{-7}$ for 1000 epochs. It is obvious that RRBF gives better convergence speed than all other networks.

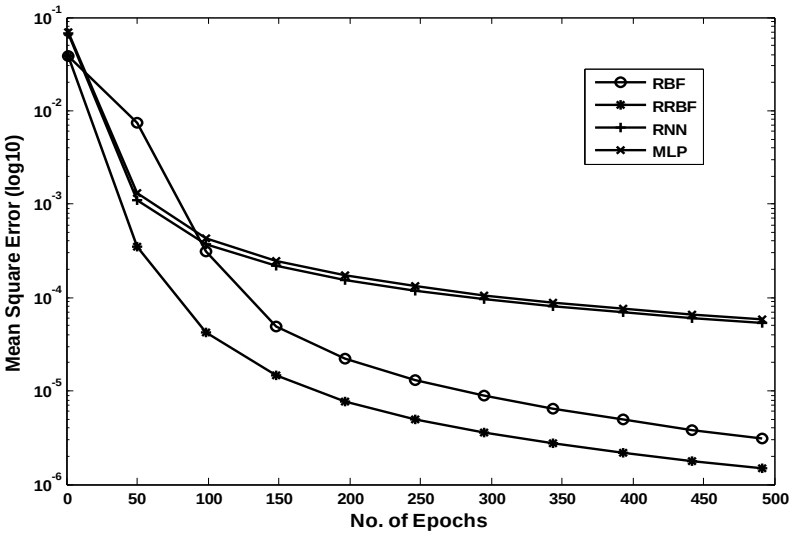

(a)

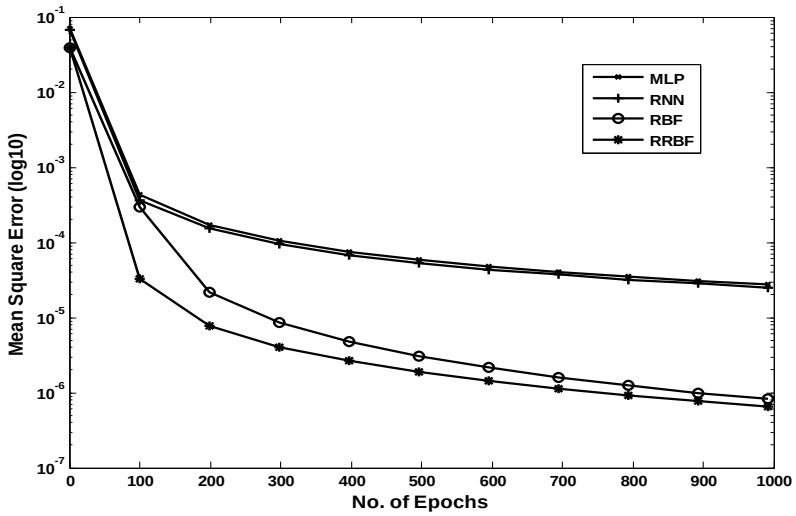

(b)

Figure 4.3. Mean square error curves for MLP, RNN, RBF and RRBF for 13-bit barker code (a) 500 epochs (b) 1000 epochs

4.4.2. SSR performance

The Signal to sidelobe ratio (SSR) is the ratio of main lobe amplitude to the peak sidelobe amplitude. The SSR is calculated for MLP, RNN, RBF and RRBF networks and results are compared for both 500 and 1000 epochs and are depicted in Table 4.1 and this shows that RRBF gives higher SSR than RNN, MLP and RBF. The compressed waveforms for 13-bit barker code for MLP, RNN, RBF and RRBF for 500 epochs are given in Figure 4.4.

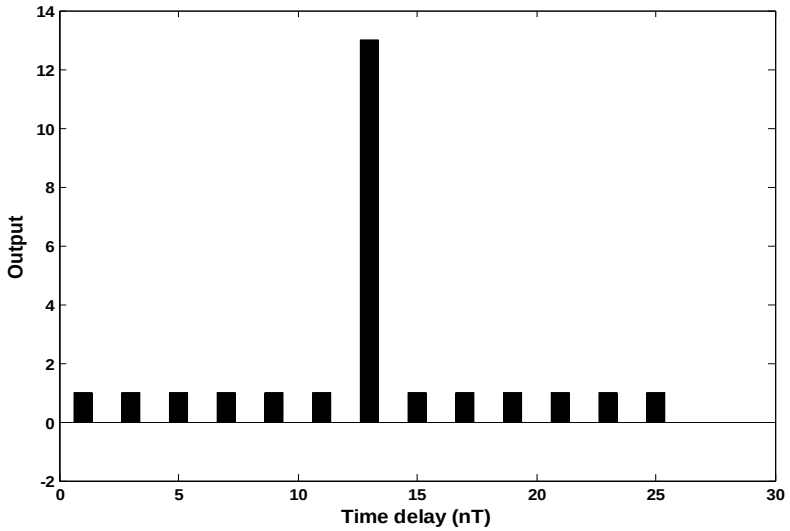

(a)

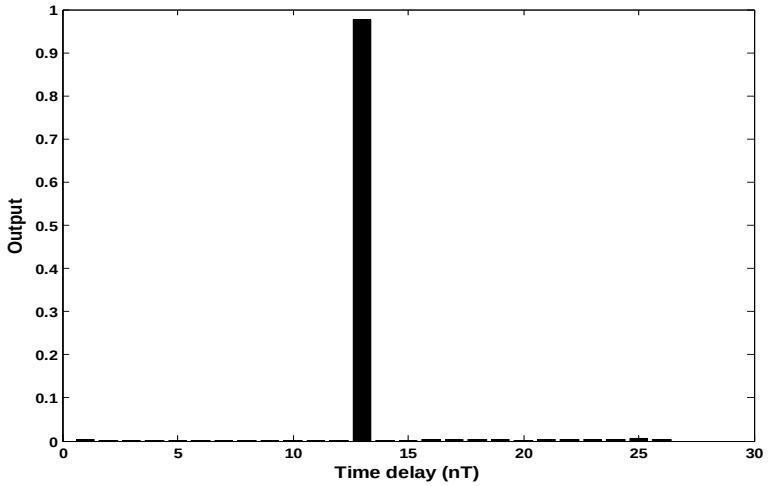

(b)

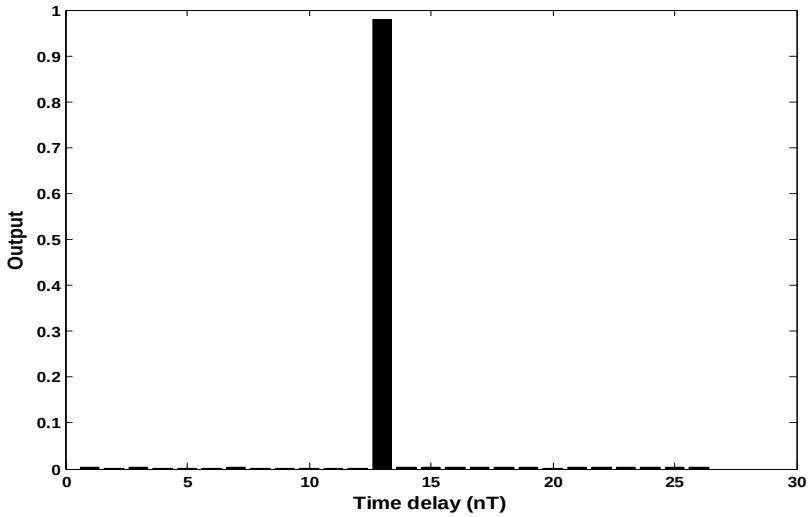
Output
Time delay (nT)
0
0.1
0.2
0.3
0.4
0.5
0.6
0.7
0.8
0.9
1
0
5
10
15
20
25
30

(c)

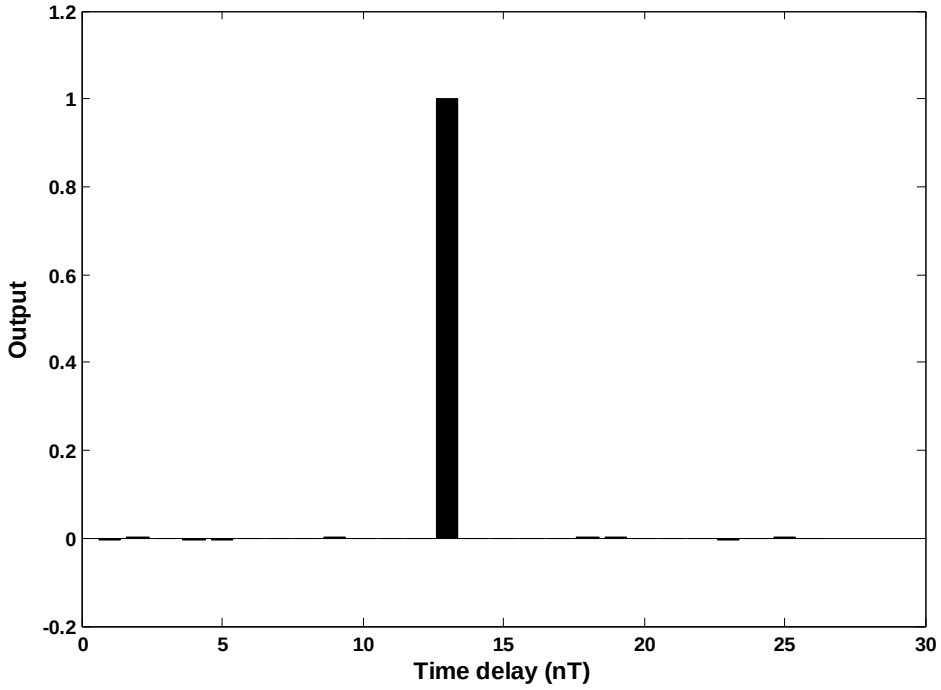
Output
Time delay (nT)
-0.2
0
0.2
0.4
0.6
0.8
1
1.2
0
5
10
15
20
25
30

(d)

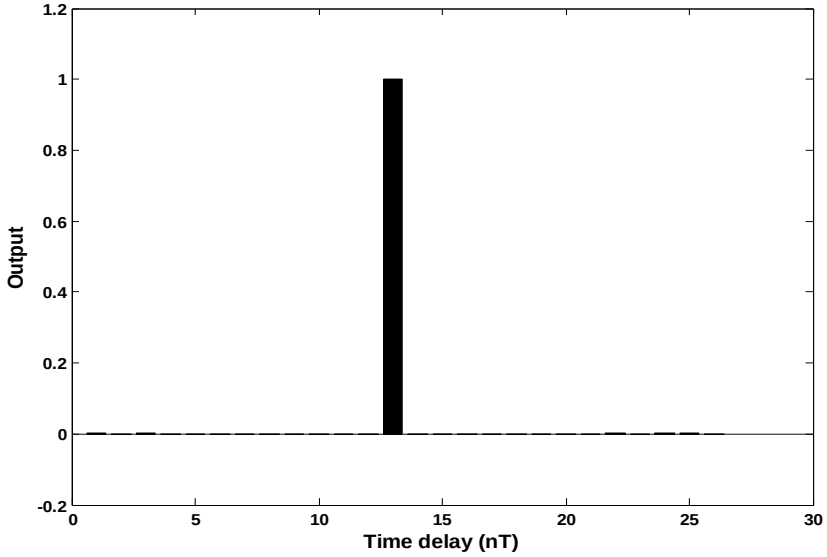

(e)

Figure 4.4. Compressed waveforms for 13-bit barker code for 500 epochs (a) ACF (b) MLP (c) RNN (d) RBF (e) RRBF

Table 4.1. SSR comparison in dB

Algorithms	SSR in dB	
	500 epochs	1000 epochs
ACF	22.27	22.27
MLP	41.63	45.13
RNN	44.53	47.91
RBF	49.78	53.51
RRBF	52.71	54.53

4.4.3. Noise performance:

The noise performance is obtained by calculating SSRs at different SNRs by adding additive white Gaussian noise to the input code. The SSRs at different SNRs for 500 and 1000 epochs are listed in Table 4.2 and 4.3 for MLP, RNN, RBF and RRBF. The noise performance at different SNRs for both 500 and 1000 epochs are shown in Figure 4.5. From all this it is clear that RRBF gives better performance than RBF and RNN, MLP.

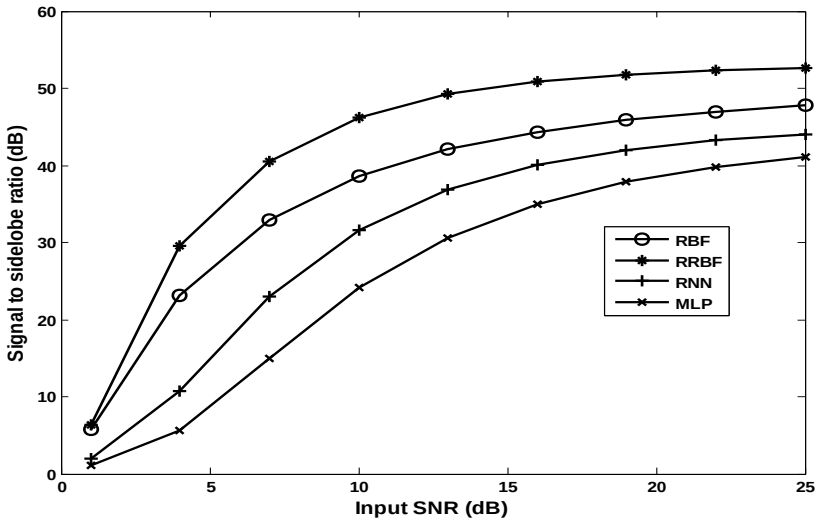

(a)

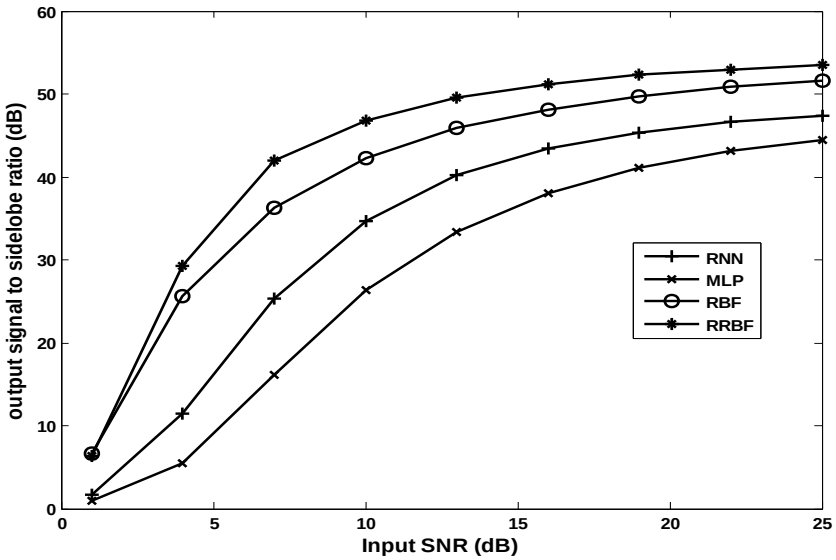

(b)

Figure 4.5. Noise performance at different SSRs for 13-bit barker code (a) 500 epochs (b) 1000 epochs

Table 4.2. Noise performance at different SSRs for 500 epochs

Algorithms	SNR=5dB	10dB	15dB	20dB	25dB
ACF	8.39	13.08	16.38	18.61	20.08
MLP	8.61	24.09	33.72	38.56	41.04
RNN	14.95	31.66	39.15	42.45	44.04
RBF	27.01	38.62	43.67	46.27	47.77
RRBF	34.05	46.25	50.47	51.99	52.58

Table 4.3. Noise performance at different SSRs for 1000 epochs

Algorithms	SNR=5dB	10dB	15dB	20dB	25dB
ACF	8.39	13.08	16.38	18.61	20.08
MLP	8.61	26.30	36.74	41.85	44.43
RNN	16.33	34.70	42.50	45.85	47.44
RBF	29.92	42.27	47.49	50.12	51.61
RRBF	29.32	46.75	50.71	52.53	53.45

4.4.4. Doppler performance

The Doppler sensitivity is caused by phase shifting the individual elements of the input phase code. The input phase code will not match with its replica if the phase of its last element is shifted by 180°. So the input code is changed to [-1 1 1 1 1 -1 -1 1 1 -1 1 -1 1] and is fed to the network. The SSR is calculated for MLP, RNN, RBF and RRBF networks for both 500 and 1000 epochs and are tabulated in Table 4.4. The compressed waveforms for 13-bit barker code for 500 epochs under Doppler shift conditions are shown in Figure 4.6. It is shown that RRBF is more robust to Doppler shift interference than MLP, RBF and ACF.

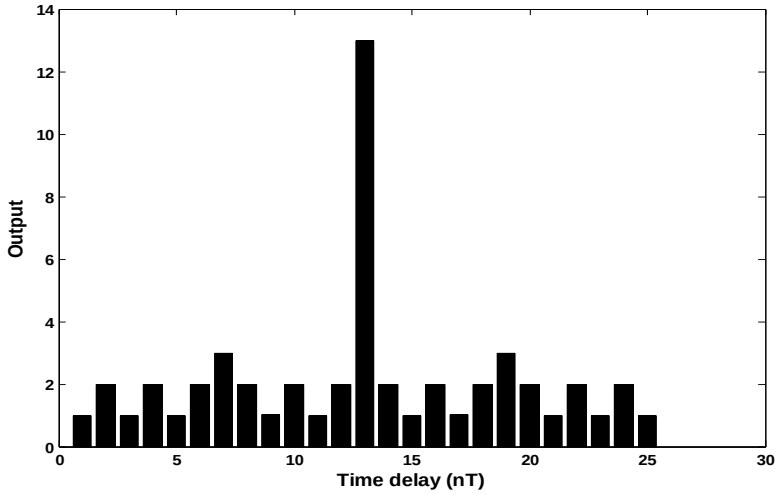
Output
Time delay (nT)
0
2
4
6
8
10
12
14
0
5
10
15
20
25
30

(a)

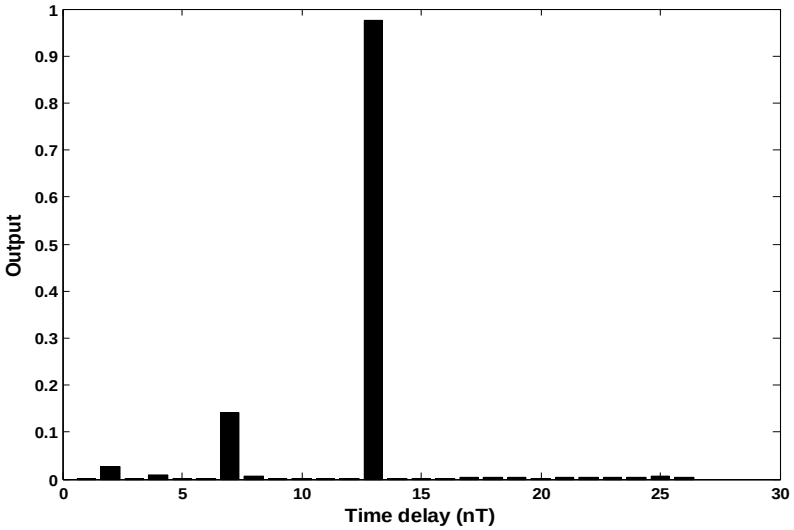
Output
Time delay (nT)
0
0.1
0.2
0.3
0.4
0.5
0.6
0.7
0.8
0.9
1
0
5
10
15
20
25
30

(b)

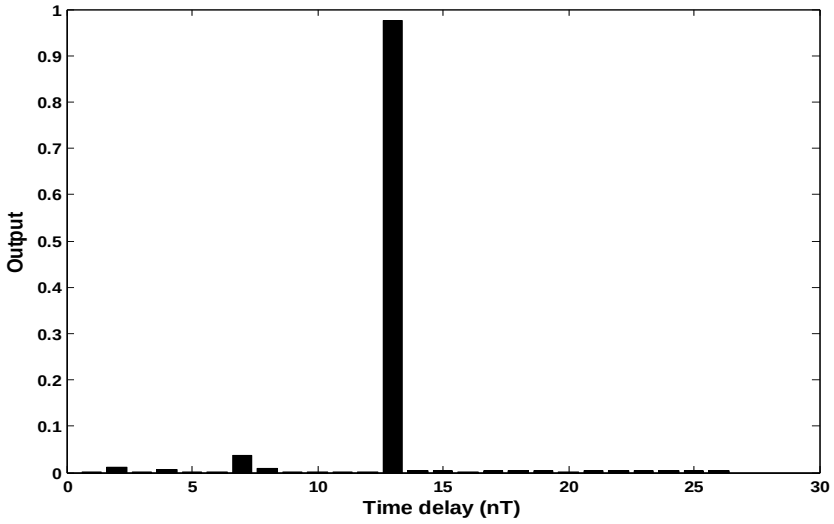
Output
Time delay (nT)
0
0.1
0.2
0.3
0.4
0.5
0.6
0.7
0.8
0.9
1
0
5
10
15
20
25
30

(c)

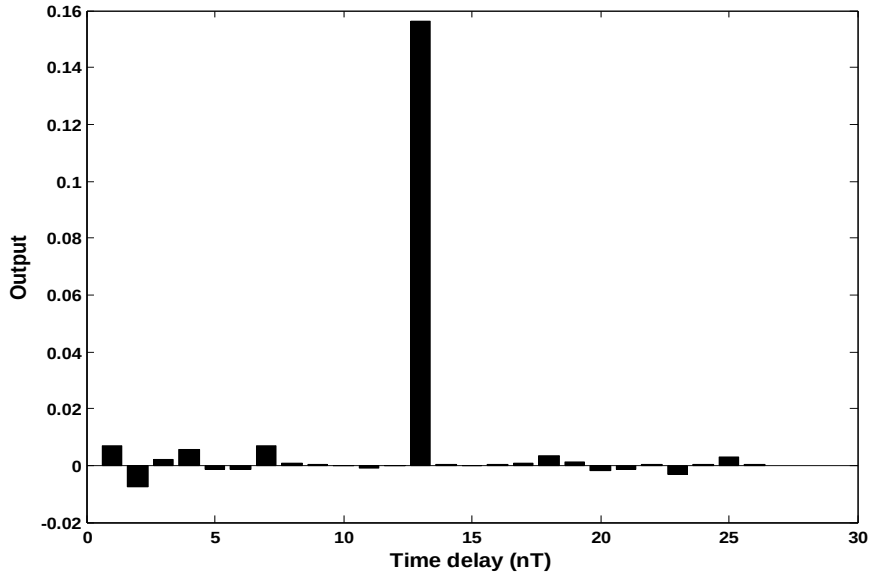
Output
Time delay (nT)
-0.02
0
0.02
0.04
0.06
0.08
0.1
0.12
0.14
0.16
0
5
10
15
20
25
30

(d)

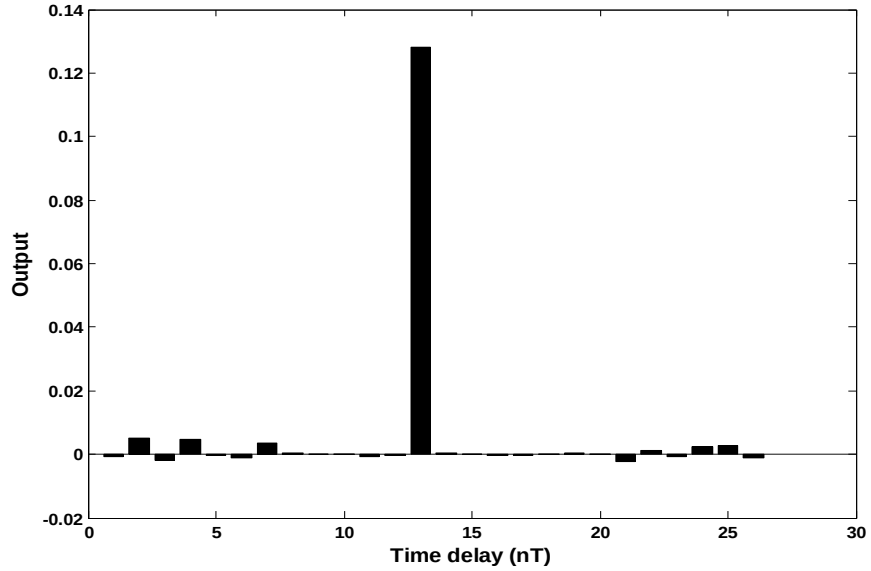

(e)

Figure 4.6. Compressed waveforms for 13-bit barker code under Doppler shift conditions for 500 epochs (a) ACF (b) MLP (c) RNN (d) RBF (e) RRBF

Table 4.4. Doppler shift performance in dB

Algorithms	SSR in dB	
	500 epochs	1000 epochs
ACF	12.74	12.74
MLP	15.06	16.38
RNN	25.78	27.68
RBF	26.56	31.63
RRBF	28.23	32.06

4.5. Summary

In this chapter, the concepts of RBF, and RRBF are discussed. The RBF and proposed RRBF network are used for pulse radar detection to compress the unwanted self-clutter sidelobes. In the simulations, error performance, SSR performance, noise performance and Doppler shift performances are done for RBF and RRBF networks and are compared with MLP, RNN and ACF algorithms. From simulation results it is clear that the recurrent RBF gives better results compared to MLP, RNN and RBF. The error converges fast in case of

RRBF than in MLP, RNN and RBF. The calculated SSR is higher in case of RRBF than MLP, RNN, RBF and traditional algorithms like ACF algorithm. Simulation results also demonstrate that RRBF yields better noise performance at different SSRs than MLP, RNN, RBF and ACF. The RRBF network is very robust to Doppler shift interference than MLP, RNN, RBF. Under Doppler shift conditions, the SSR is calculated as 15.06dB for MLP, 25.78dB for RNN, 26.56dB for RBF, whereas RRBF gives better SSR of 28.23dB for 500 epochs.

Chapter – 5

A Study of Polyphase Codes and Their Sidelobe Reduction Techniques

5.1. Introduction

If the phases of subpulses in phase coded pulse compression are other than the binary phases of 0 and π, then the phase codes are called polyphase codes [5.1]. They have lower sidelobes than binary codes and are more Doppler tolerant if the Doppler frequencies are not too large. Frank proposed a polyphase code with good non-periodic correlation properties and named the code as Frank code [5.4]. Kretscher and Lewis proposed different variants of Frank polyphase codes called p-codes which are more tolerant than Frank codes to receiver bandlimiting prior to pulse compression [5.5, 5.6]. Lewis has proven that the sidelobes of polyphase codes can be substantially reduced after reception by following the autocorrelator with two sample sliding window subtractor for Frank and P1 codes and TSSWA for P3 and P4 codes.

This chapter is about the different polyphase codes and their properties. First the golay complementary codes are discussed followed by the discussion polyphase shift keying techniques which contain Frank, P1, P2, P3, P4 codes. For each code, the phase characteristics, autocorrelation properties and doppler properties are examined. Also the TSSWA and double TSSWA after autocorrelator are described in detail and are applied for P4 code. The weighting techniques are applied using Kaiser Bessel and Hamming windows and the results are compared.

5.2. Golay Complementary codes

Golay complementary codes [5.2] have properties that are useful in radar and communications systems. The sum of autocorrelations of each of a Golay complementary code pair is a delta function. This property can be used for the complete removal of sidelobes from radar signals, by transmitting each code, match–filtering the returns and combining them.

Consider two discrete binary sequences of length N, p1(n) and p2(n), are termed Golay complementary sequences if the sum of their autocorrelations is zero except at zero lag, *i.e.*

$$R_{p_1}(k) + R_{p_2}(k) = 2N\delta(k) \tag{5.1}$$

Where the R_{p1}, R_{p2} are the autocorrelations of p_1 and p_2 codes respectively. The properties of golay complementary codes are as follows,

$$p_1(n),\ p_2(n)\ \in \{1,-1\},\ n = 1,2,\dots\ N \tag{5.2}$$

$$R_{p_1}(k) + R_{p_2}(k) = 2N, k = 0 \tag{5.3}$$

$$R_{p_1}(k) = -R_{p_2}(k),\ k \neq 0 \tag{5.4}$$

$$R_{p_1}(k)^2 = R_{p_1}(k)^2 \tag{5.5}$$

It is also the case that

$$R_{p_1}(2k) = R_{p_2}(2k), \forall\ k \neq 0 \tag{5.6}$$

provided that the Golay sequences are constructed in a standard manner from a length–2 seed and are not permuted. A length–8 Golay pair and its complementary property is illustrated in Figure 5.1.

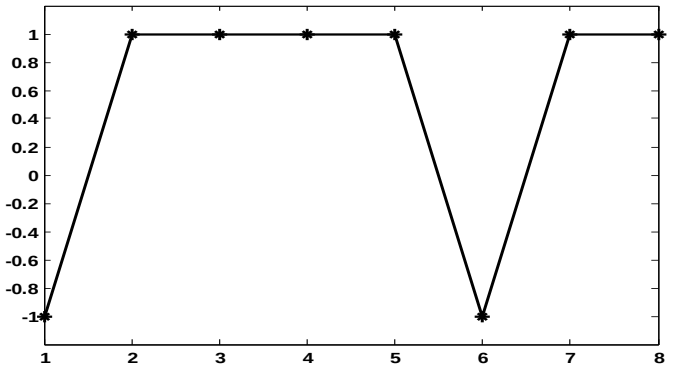

(a)

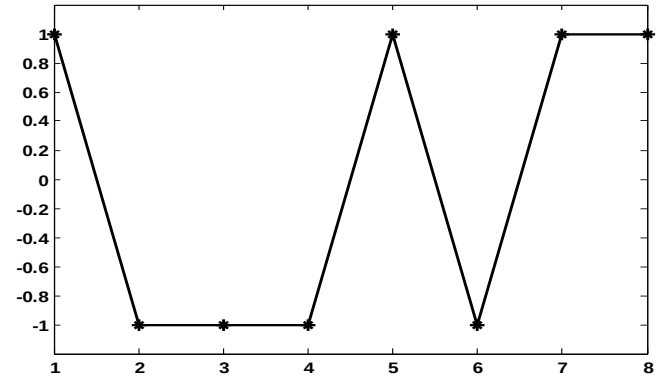

(b)

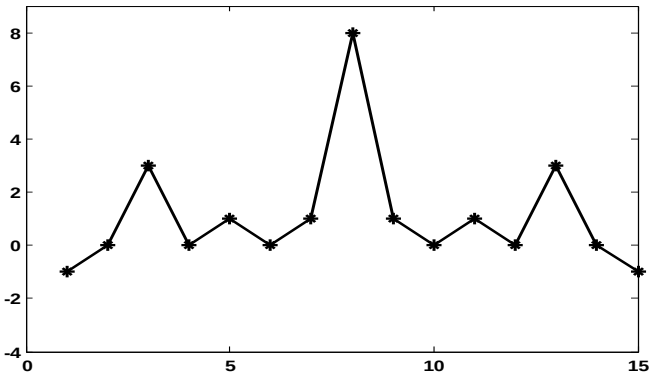

(c)

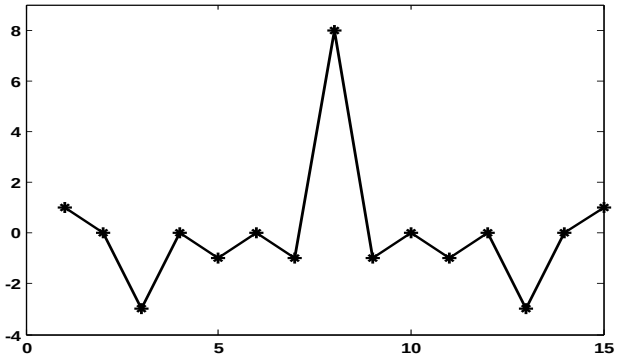

(d)

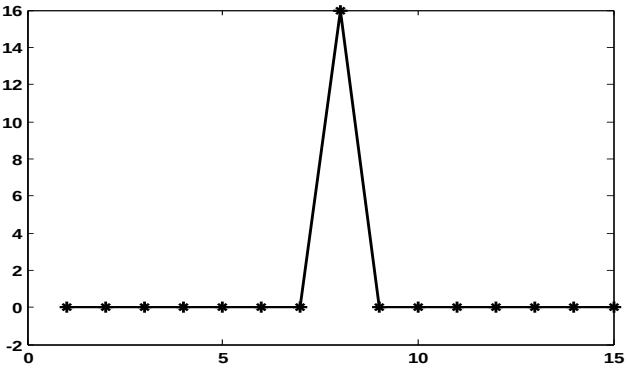

(e)

Figure 5.1. (a, b) Golay complementary codes (b, c) their respective autocorrelation functions (e) sum of the autocorrelations

Individual Golay sequences have relatively flat spectra. The peak–to–mean envelope power ratio of a Golay sequence can be shown to be bounded by length of the sequence [2]. This has application in OFDM power control.

5.2.1. Modified Golay Complementary Code

Let $p_1(n)$ and $p_2(n)$ be a Golay complementary pair. The modification is done for p2 code and the modified code q in terms of p_2 is expressed as

$$q(n) = p_2(n).e^{i\frac{\pi}{2}n} \tag{5.7}$$

The autocorrelations of original code p_2 and modified code q are related as follows

$$R_q(k) = R_{p_2}(k)e^{i\frac{\pi}{2}k} \tag{5.8}$$

The square of autocorrelation functions of p_1, p_2, and q are related as follows

$$R_q(k)^2 = R_{p_2}(k)^2.e^{i\pi k}$$

$$= \begin{cases} -R_{p_1}(k)^2, & if\ k\ is\ odd \\ 0, & if\ k\ is\ even, k \neq 0 \\ R_{p_1}(k)^2, & if\ k = 0 \end{cases} \tag{5.9}$$

And hence

$$R_q(k)^2 + R_{p_1}(k)^2 = 2N^2\delta(k) \tag{5.10}$$

From the above equation it is evident that the square of autocorrelation functions of p_2 and q are complementary to each other. The complementarity of the modified golay code with the other code and its sum of squared autocorrelation functions are illustrated in Figure 5.2.

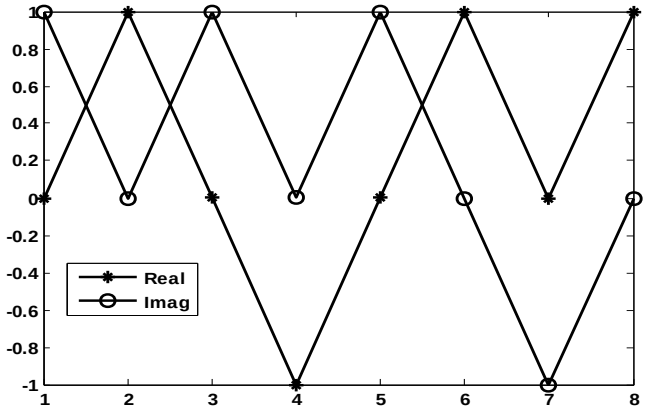

(a)

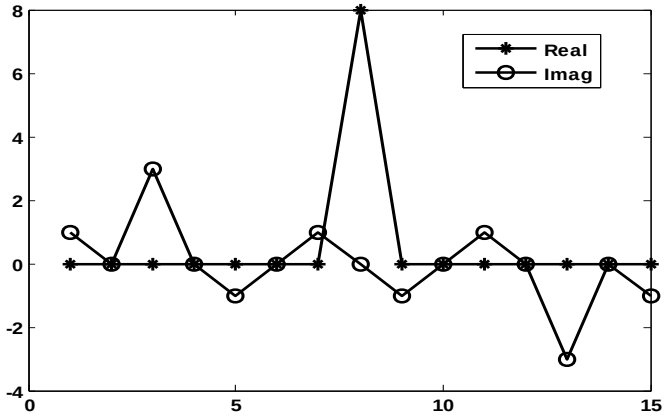

(b)

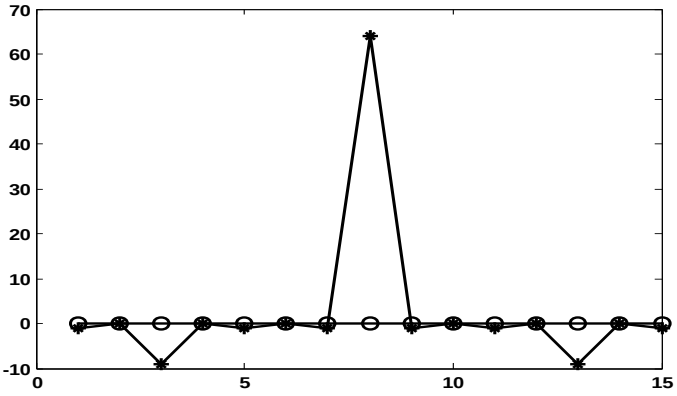

(c)

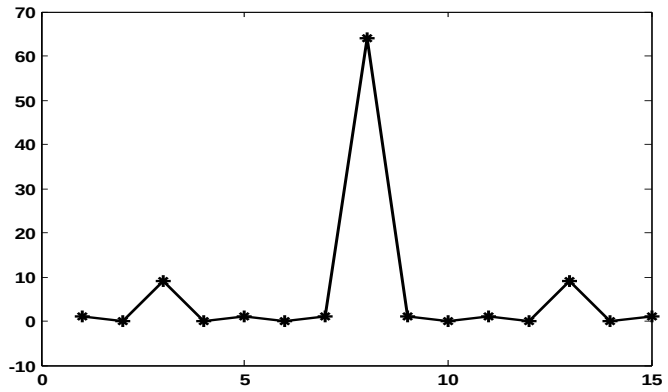

(d)

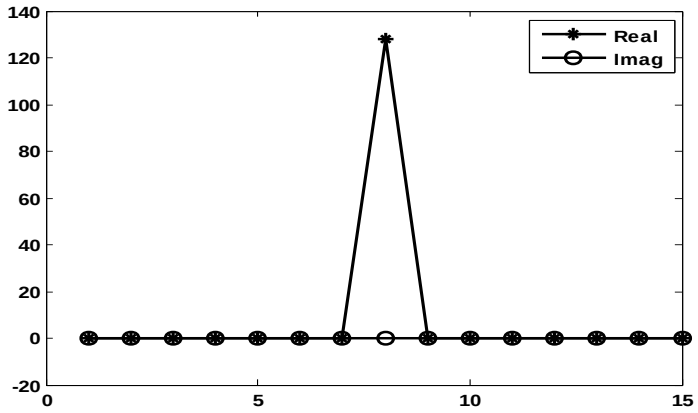

(e)

Figure 5.2. (a) Modified Golay code q (b) its autocorrelation function (c) its squared autocorrelation (d) squared autocorrelation of p_2 (e) sum of squared autocorrelations of q and p_2

Hence if both the sequences are multiplied by $e^{i\frac{\pi}{2}n}$ then they are complementary to each other but only one of the codes is multiplied by $e^{i\frac{\pi}{2}n}$ results in a pair which is complementary in the square [5.3].

Even though the Golay complementary codes provide complete sidelobe cancellation, they are not tolerant of doppler shifts caused by targets moving relative to the radar. Hence we go for polyphase codes that has many applications which include low sidelobe levels, good doppler tolerance for search radar applications and ease of implementation.

5.3. Polyphase codes

The codes that use any harmonically related phases based on a certain fundamental phase increment are called Polyphase codes. Polyphase codes exhibit better Doppler tolerance for broad range-Doppler coverage than do the biphase codes, and they exhibit relatively good side lobe characteristics.

Polyphase compression codes have been derived from step approximation to linear frequency modulation waveforms (Frank, P1, P2) and linear frequency modulation waveforms (P3, P4). These codes are derived by dividing the waveform into subcodes of equal duration, and using phase value for each subcode that best matches the overall phase trajectory of the underlying waveform. In this section the polyphase codes namely Frank, P1, P2, P3, P4 codes and their properties are described.

5.3.1. Frank Code

The Frank code is derived from a step approximation to a linear frequency modulation waveform using N frequency steps and N samples per frequency [5.4]. Hence the length of Frank code is N^2. The Frank coded waveform consists of a constant amplitude signal whose carrier frequency is modulated by the phases of the Frank code.

The phases of the Frank code is obtained by multiplying the elements of the matrix A by phase ($2\pi/N$) and by transmitting the phases of row1 followed by row 2 and so on.

$$A=\begin{bmatrix} 0 & 0 & 0 & \dots & 0 \\ 0 & 1 & 2 & \dots & (N-1) \\ 0 & 2 & 4 & \dots & 2(N-1) \\ 0 & 3 & 6 & \dots & 3(N-1) \\ . & & & & \\ . & & & & \\ 0 & (N-1) & 2(N-1) & \dots & (N-1)^2 \end{bmatrix} \tag{5.11}$$

The phase of the *i*th code element in the *j*th row of code group is computed as

$$\Phi_{i,j}=\left(\frac{2\pi}{N}\right)(i-1)(j-1) \tag{5.12}$$

Where *i* and *j* ranges from 1 to N. For example, the Frank code with N = 4, by taking phase value modulo 2π is given by the sequence,

$$\phi_{4x4} = \begin{bmatrix} 0 & 0 & 0 & 0 \\ 0 & \frac{\pi}{2} & \pi & \frac{3\pi}{2} \\ 0 & \pi & 0 & \pi \\ 0 & \frac{3\pi}{2} & \pi & \frac{\pi}{2} \end{bmatrix}$$

The autocorrelation function under zero Doppler, Doppler of 0.05 and the phase values of Frank code with length 100 are given in Figure 5.3.

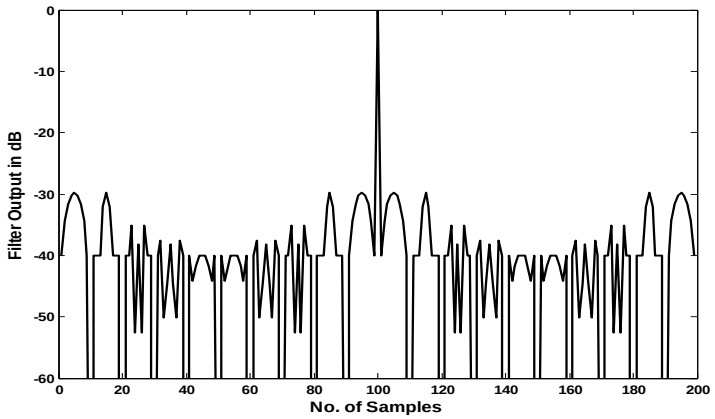

(a)

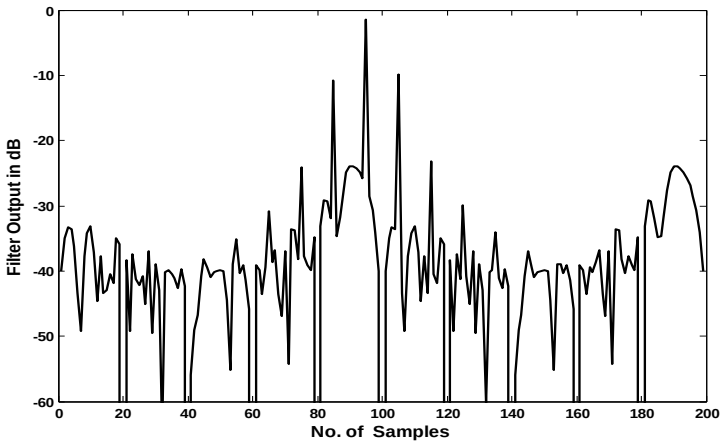

(b)

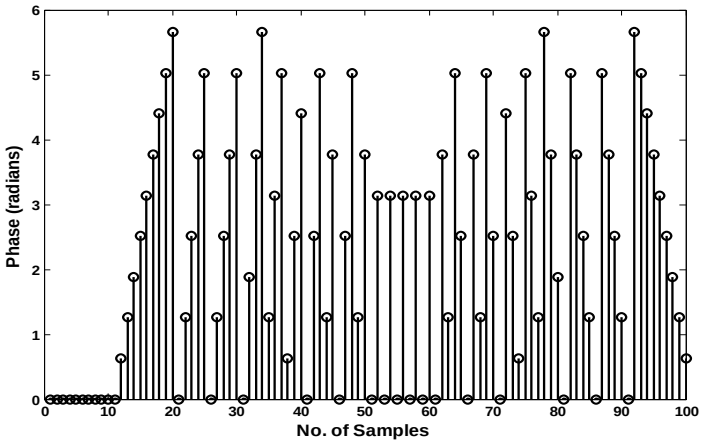

(c)

Figure 5.3. Frank Code for length 100 (a) Autocorrelation under zero Doppler shift (b) Autocorrelation under doppler = 0.05 (c) phase values

From the above figure it is evident that the Frank code has the largest phase increments from sample to sample in the center of the code. Hence, when the code is passed through a bandpass amplifier in a radar receiver, the code is attenuated more in the center of the waveform. This attenuation tends to increase the sidelobes of the Frank code ACF. Hence it is very intolerant to precompression bandlimiting. But comparing with binary phase codes, the Frank code has a peak sidelobe level (PSL) ratio of -29.79dB which is approximately 10 dB better than the best pseudorandom codes [5.1].

In the presence of Doppler shift, the autocorrelation function of Frank codes degrades at much slower rate than that for binary codes, however the peak shifts in position rapidly and a range error occurs due to this shift. The correlation under Doppler frequency f_d is obtained by correlating the transmitted one with received one multiplied by $e^{-j2\pi f_d T}$, where T is the length of the code. The PSL value under Doppler of 0.05 is calculated as -8.42dB.

5.3.2. P1 Code

The P1, P2, P3, P4 codes are obtained by the modified versions of the Frank code, with the dc frequency term in the middle of the pulse instead of at the beginning. P1 code is derived

by placing the synchronous oscillators at the center frequency of the step chirp IF waveform and sampling the baseband waveform at the Nyquist rate [5.5].

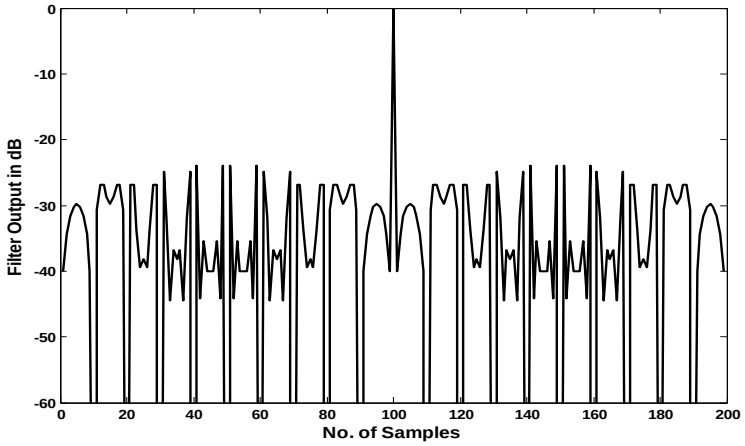

(a)

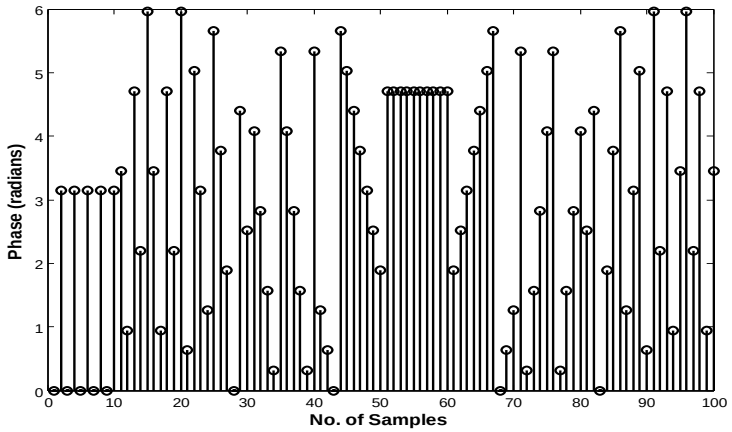

(b)

Figure 5.4. P1 Code for length 100 (a) its Autocorrelation (b) its phase values

The P1 code has N^2 elements and the phase of *i*th element of the *j*th group is represented as

$$\Phi_{i,j} = -\left(\frac{\pi}{N}\right)[N-(2j-1)][(j-1)N+(i-1)] \tag{5.13}$$

Where *i* and *j* are integers ranges from 1 to N. For example, the P1 code with N = 4, by taking phase value modulo 2π is given by the sequence,

$$\phi_{4x4} = \begin{bmatrix} 0 & \pi & 0 & \pi \\ \frac{5\pi}{4} & \frac{3\pi}{4} & \frac{\pi}{4} & \frac{7\pi}{4} \\ \frac{\pi}{2} & \frac{\pi}{2} & \frac{\pi}{2} & \frac{\pi}{2} \\ \frac{7\pi}{4} & \frac{\pi}{4} & \frac{3\pi}{4} & \frac{5\pi}{4} \end{bmatrix}$$

The autocorrelation function and the phase values of P1 code with length 100 are given in Figure 5.4. The PSL value is obtained as -23.99dB. P1 code has the highest phase increments from sample to sample at the two ends of the code. Thus, when waveforms phase coded with these codes are passed through band pass amplifiers in a radar receiver, P1 code is attenuated most heavily at the two ends of the waveform. This reduces the sidelobes of the P1 code autocorrelation function. Hence this exhibits relatively low sidelobes than Frank code. This results that P2 code is very precompression bandwidth tolerant than Frank code. Also, the P1 code has an autocorrelation function magnitude which is identical to the Frank code for zero Doppler shift.

5.3.3. P2 Code

The P2 code has the same phase increments within each phase group as the P1 code, except that the starting phases are different [5.1]. The P2 code has N^2 elements and the phase of *i*th element of the *j*th group is represented as

$$\Phi_{i,j} = \left(\frac{\pi}{2N}\right)[N - 2i + 1][N - 2j + 1] \tag{5.14}$$

Where *i* and *j* are integers ranges from 1 to N.The value of N should be even in order to get low autocorrelation sidelobes. An odd value of N results in high autocorrelation sidelobes. For example, the P2 code with N = 4, by taking phase value modulo 2π is given by the sequence,

$$\phi_{4x4} = \begin{bmatrix} \frac{9\pi}{8} & \frac{3\pi}{8} & \frac{13\pi}{8} & \frac{7\pi}{8} \\ \frac{3\pi}{8} & \frac{\pi}{8} & \frac{15\pi}{8} & \frac{13\pi}{8} \\ \frac{13\pi}{8} & \frac{15\pi}{8} & \frac{\pi}{8} & \frac{3\pi}{8} \\ \frac{7\pi}{8} & \frac{13\pi}{8} & \frac{3\pi}{8} & \frac{9\pi}{8} \end{bmatrix}$$

The autocorrelation function under zero Doppler, Doppler of 0.05 and the phase values of P2 code with length 100 are given in Figure 5.5.

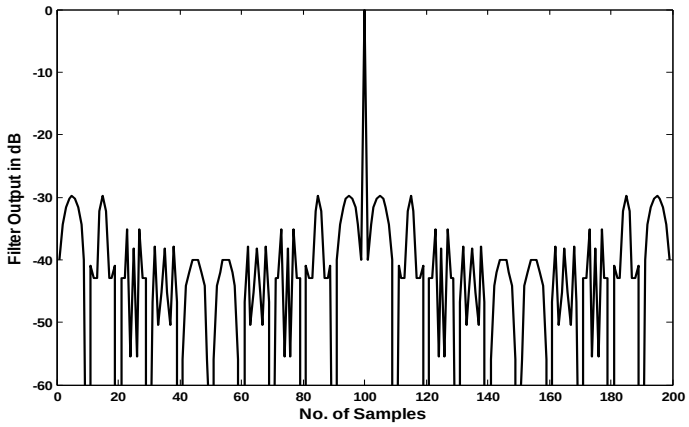

(a)

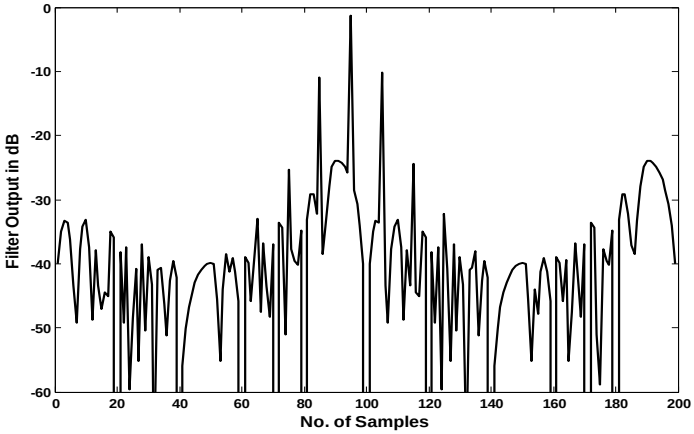

(b)

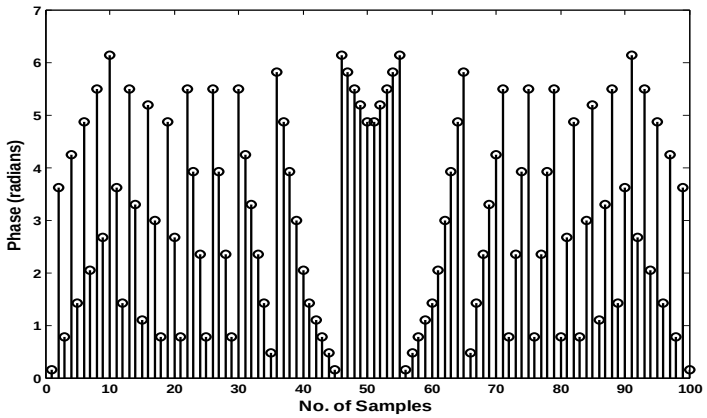

(c)

Figure 5.5. P2 Code for length 100 (a) Autocorrelation under zero doppler shift (b) Autocorrelation under doppler = 0.05 (c) phase values

The peak sidelobes of the P2 code are the same as the Frank code for zero Doppler case and the mean square sidelobes of the P2 code are slightly less. The value of PSL obtained as -29.79dB which is same as that of Frank code. Under Doppler of 0.05 the PSL value is computed as -8.79dB which is slightly lower than that of Frank code. The phase changes in P2 code are largest towards the end of the code.

The significant advantage of the P1 and P2 codes over the Frank code is that they are more tolerant of receiver band limiting prior to pulse compression. But P1 and P2 suffers from high PSL value. PSL value is obtained by the ratio of peak sidelobe amplitude to the main lobe amplitude. To obtain low PSL values, we go for P3 and P4 codes.

5.3.4. P3 Code

The P3 code is conceptually derived by converting a linear frequency modulation waveform to baseband using a local oscillator on one end of the frequency sweep and sampling the inphase I and quadrature Q video at the Nyquist rate [5.6].

The phase sequence of the P3 signal is given by

$$\Phi_i = \frac{\pi}{N}\,(i-1)^2 \tag{5.15}$$

Where i varies from 1 to N and N is the compression ratio. For example, the P3 code with N = 16, by taking phase value modulo 2π is given by the sequence,

$$\Phi_{16} = \left[0 \quad \frac{\pi}{16} \quad \frac{4\pi}{16} \quad \frac{9\pi}{16} \quad \pi \quad \frac{25\pi}{16} \quad \frac{4\pi}{16} \quad \frac{17\pi}{16} \quad 0 \quad \frac{17\pi}{16} \quad \frac{4\pi}{16} \quad \frac{25\pi}{16} \quad \pi \quad \frac{9\pi}{16} \quad \frac{4\pi}{16} \quad \frac{\pi}{16} \right]$$

The autocorrelation function and the phase values of P3 code with length 100 are given in Figure 5.6. The PSL value is obtained as -26.32dB.

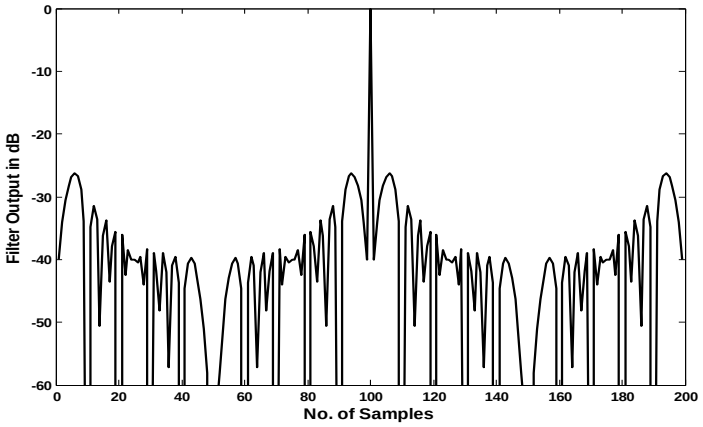

(a)

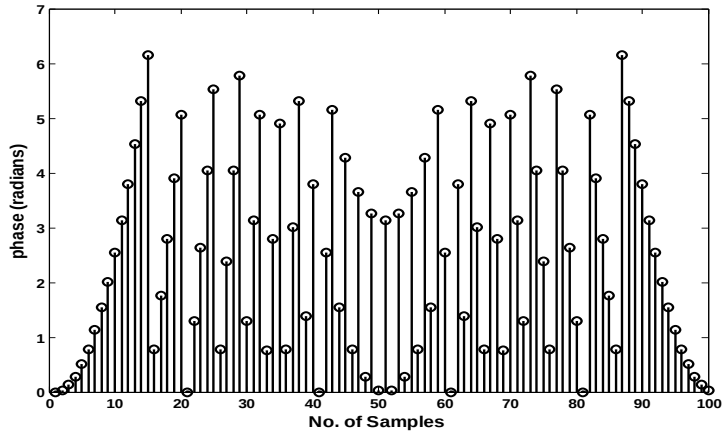

(b)

Figure 5.6. P3 Code for length 100 (a) its Autocorrelation (b) its phase values

The peak side lobe ratio for P3 code is a bit larger than the Frank, P1, P2 codes. In the P3 code, the largest phase increments occur at the center of the code. Hence the P3 code is not

precompression bandwidth limitation tolerant but is much more Doppler tolerant than the Frank or P1 and P2 codes.

5.3.5. P4 Code

P4 code is derived from conceptual coherent double sideband detection of a linear frequency modulation waveform and sampling at the Nyquist rate [5.6]. The phase sequence of the P4 signal is given by

$$\Phi_i = \frac{\pi}{N}(i-1)(i-N-1) \tag{5.15}$$

Where i varies from 1 to N and N is the compression ratio. For example, the P4 code with N = 16, by taking phase value modulo 2π is given by the sequence,

$$\Phi_{16} = \left[0 \quad \frac{17\pi}{16} \quad \frac{4\pi}{16} \quad \frac{25\pi}{16} \quad \pi \quad \frac{9\pi}{16} \quad \frac{4\pi}{16} \quad \frac{\pi}{16} \quad 0 \quad \frac{\pi}{16} \quad \frac{4\pi}{16} \quad \frac{9\pi}{16} \quad \pi \quad \frac{25\pi}{16} \quad \frac{4\pi}{16} \quad \frac{17\pi}{16} \right]$$

The autocorrelation function under zero Doppler, Doppler of 0.05 and the phase values of P4 code with length 100 are given in Figure 5.7. The PSL value is obtained as -26.32dB under zero Doppler, and -22.31dB under Doppler of 0.05 which are similar to P3 code.

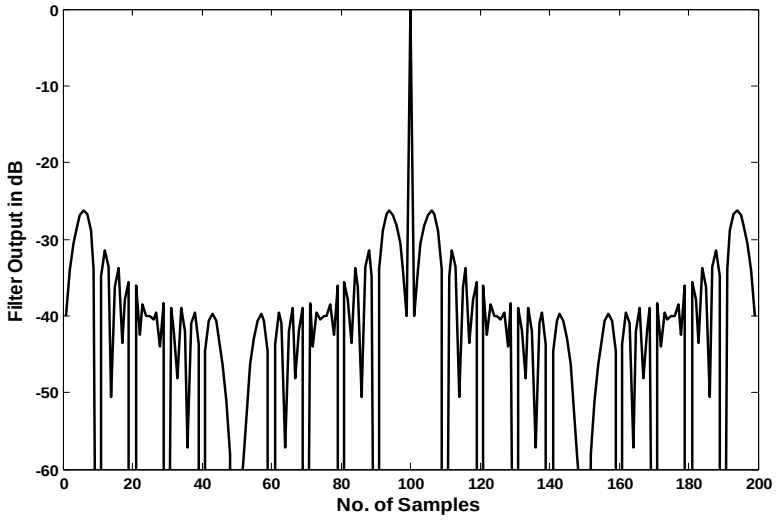

(a)

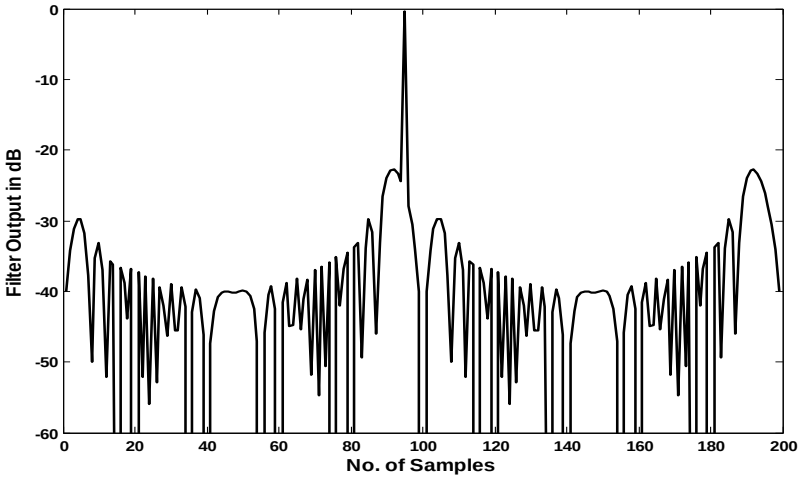

(b)

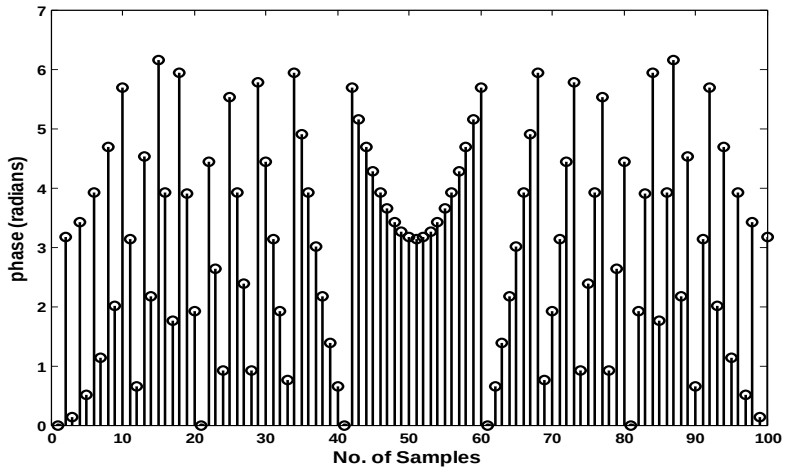

(c)

Figure 5.7. P4 Code for length 100 (a) Autocorrelation under zero doppler shift (b) Autocorrelation under doppler = 0.05 (c) phase values

The largest phase increments from code element to code element are on the two ends of the P4 code but are in the middle of the P3 code. Thus the P4 code is more precompression bandwidth limitation tolerant but has same Doppler tolerance than the P3 code.

5.4. Two Sample Sliding Window Adder (TSSWA)

TSSWA is applied for polyphase codes inorder to reduce the PSL values. It is a new type of pulse compression technique that compresses the pulse to the width of several subpulses and not to the width of single subpulse by reducing bandwidth [5.8].

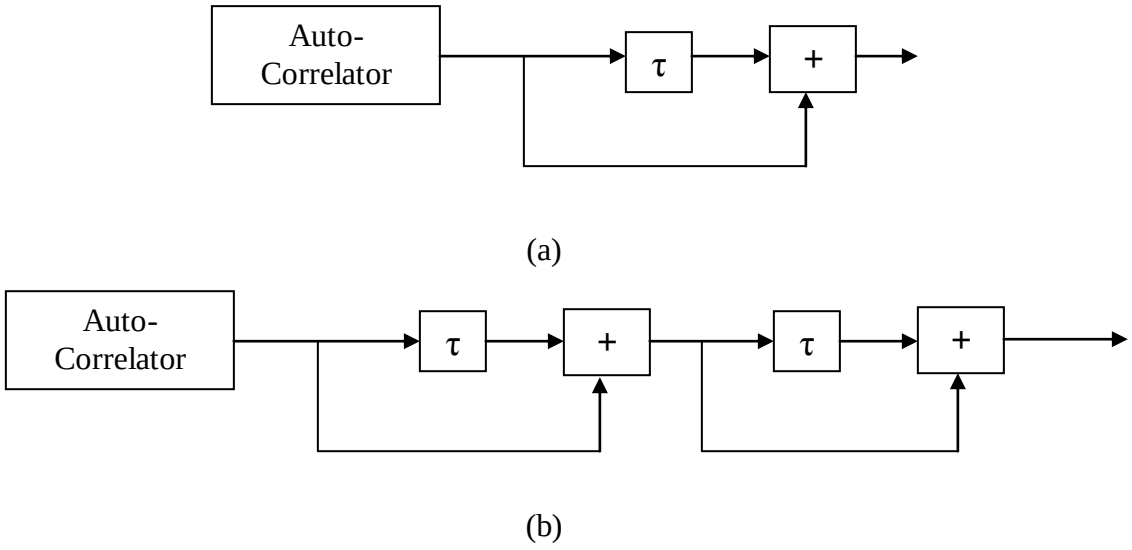

Figure 5.8. (a) Auto-correlator followed by single TSSWA (b) Auto-correlator followed by double TSSWA

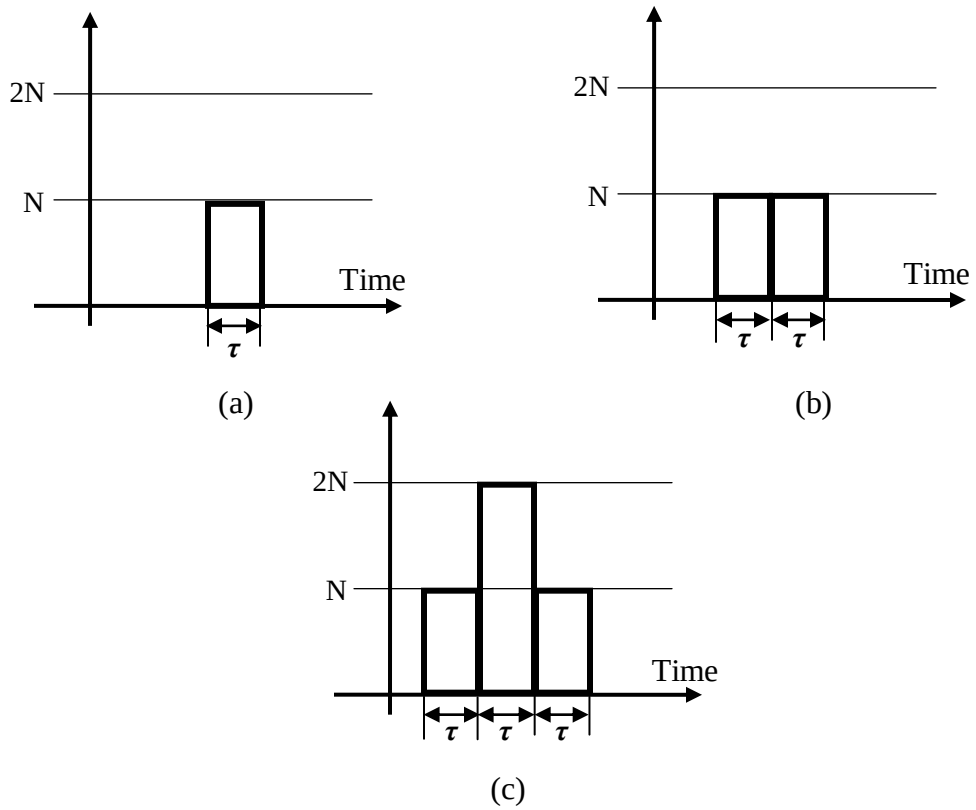

Figure 5.9. (a) Correlator output (b) Single TSSWA output (c) Double TSSWA output

The TSSWA is added after the autocorrelator of the code. The block diagram of autocorrelator followed by single TSSWA and double TSSWA are shown in Figure 5.8. The spectrum bandwidth of the coded signal is approximately the inverse of the subpulse width τ in the conventional autocorrelation output which is given in Figure 5.9(a). Hence the pulse is then compressed to a single subpulse. The function of TSSWA is to divide the signal into two, delay one of them by τ and add it to the other one [5.8]. The output of the autocorrelator followed by a single TSSWA is given in Figure 5.9(b).

The compressed width after single TSSWA will be 2τ. Further if again one more TSSWA is added to single TSSWA output then autocorrelator followed by double TSSWA is formed and its output has compressed width of 3τ as shown in Figure 5.9(c). From the spectral point of view, the TSSWA is carried out once, if the weighting function $(1+\cos\omega\tau)$ is multiplied by the spectral intensity of the input signal so that bandwidth becomes narrowed. For double TSSWA, the weighting function $(1+\cos\omega\tau)^2$ is multiplied by the spectral intensity of the input signal so that the signal bandwidth becomes narrower and so on.

In this section, single TSSWA and double TSSWA are applied for P4 code of length 100. The autocorrelation output, the output of autocorrelation followed by single TSSWA, followed by double TSSWA are shown in Figure 5.10. The corresponding PSL values are depicted in Table 5.1.

Table 5.1. Comparison of PSL values

P4 code (N=100)	PSL (in dB)
ACF	-26.32
Single TSSWA output	-34.00
Double TSSWA output	-34.28

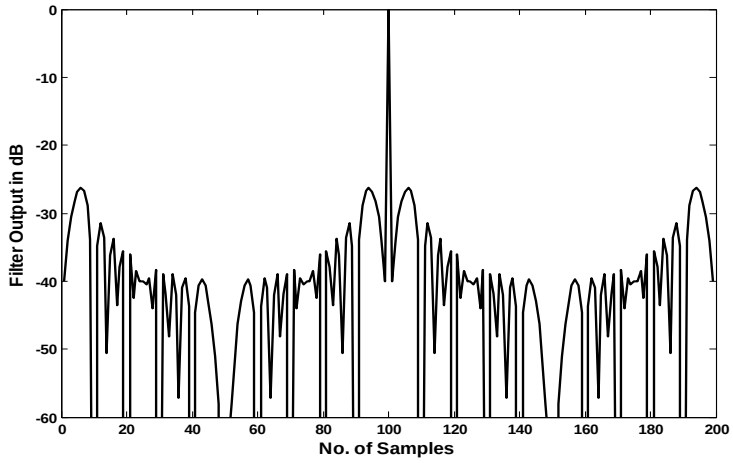
Filter Output in dB
No. of Samples
0
-10
-20
-30
-40
-50
-60
0
20
40
60
80
100
120
140
160
180
200

(a)

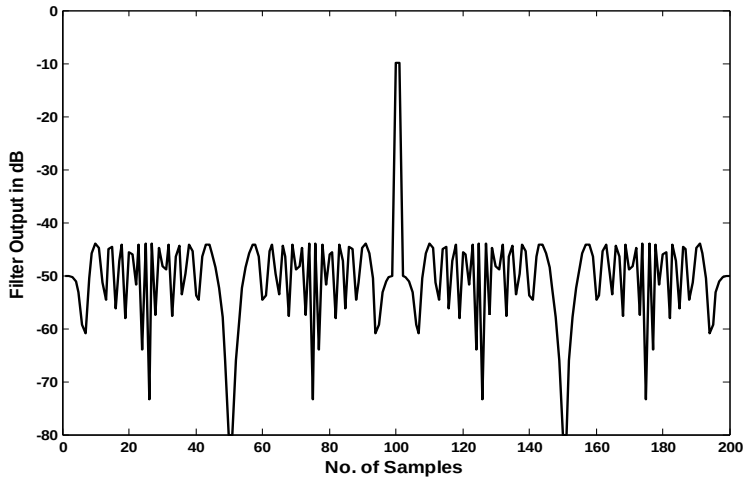
Filter Output in dB
No. of Samples
0
-10
-20
-30
-40
-50
-60
-70
-80
0
20
40
60
80
100
120
140
160
180
200

(b)

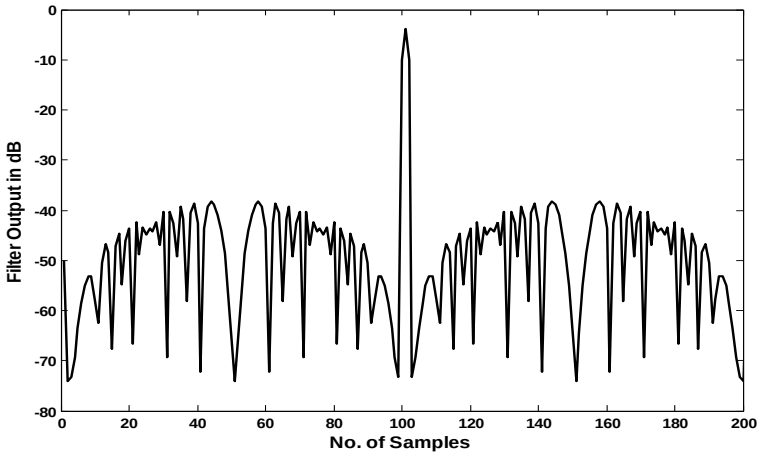
Filter Output in dB
No. of Samples
0
-10
-20
-30
-40
-50
-60
-70
-80
0
20
40
60
80
100
120
140
160
180
200

(c)

Figure 5.10. 100-element P4 code (a) Autocorrelation output (b) Single TSSWA output after autocorrelator (c) Double TSSWA output after autocorrelator

5.5. Weighting Techniques for Polyphase Codes

There will be significant reduction in sidelobes and PSL values than TSSWA by implementing time weighting function to the signal code. This sidelobe reduction technique can be analysed in two ways [5.9], one is matched weighting with weighting window at the transmitter and the receiver and two is mismatched weighting, where amplitude weighting is performed only at receiver site . In this section, simulations are done using mismatched weighting.

In this section, Kaiser-Bessel time weighting function is analysed due to β parameter and its influence on sidelobe suppression and efficiency in Doppler shift domain, as well. The PSL and integrated sidelobe level (ISL) values are compared for different weighting functions such as Kaiser-Bessel, hamming, hanning, blackmann etc.

Inorder to determine the quality of a coding scheme and sidelobes suppression method, the peak sidelobe level (PSL) and the integrated sidelobe level (ISL) of ACF are computed [5.16] and can be defined (in decibels) as follows

$$PSL_{[dB]} = 10\log_{10}\left[\frac{\max R^2(k)}{R^2(M)}\right] \tag{5.16}$$

$$ISL_{[dB]} = 10\log\sum_{k=1}^{2M-1}\frac{R^2(k)}{R^2(M)} \tag{5.17}$$

Where k is the index for the points in the ACF, R(M) is the peak of the ACF at k = M, R(k) is ACF for all of the output range sidelobes except that at k = M.

The PSL is bounded by the code length N and its level is approximately given (in decibels) by

$$PSL_{[dB]} = -(0\log_{10} N + 6) \tag{5.18}$$

Here the weighting techniques are applied to P4 code. The PSL's of the P4 codes diminish as the number of code element N (or equivalently the time-bandwidth product) increases. The PSL value for P4 code of length N=100 is -26.32dB. The Hamming window and Kaiser-Bessel windows are explained in detail and they are applied to P4 code and the values of PSL and ISL are compared.

5.5.1. Hamming Window

Hamming window belongs to the family of raised cosine windows. The window is optimized to minimize the maximum (nearest) side lobe, giving it a height of about one-fifth that of the Hann window, a raised cosine with simpler coefficients [5.19]. The coefficients of a Hamming window are computed from the following equation.

$$w(n) = 0.54 - 0.46\cos\left(2\pi\frac{n}{N}\right), \quad 0 \le n \le N \tag{5.19}$$

The 100- point hamming code is shown in Figure 5.11.

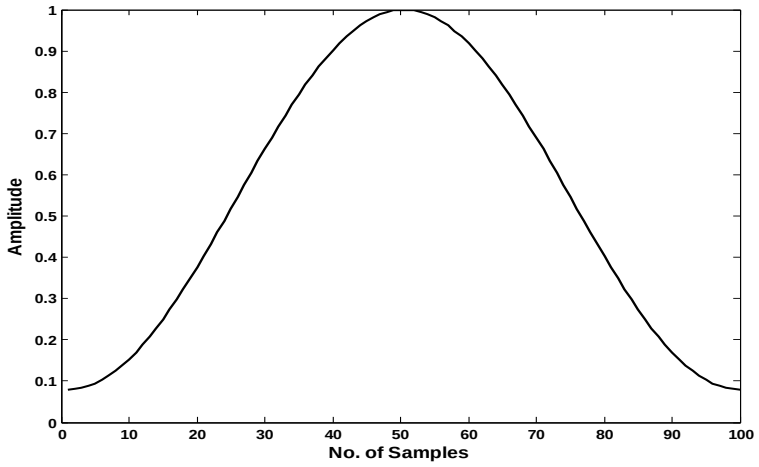

Figure 5.11. Hamming code of length 100

5.5.2. Kaiser-Bessel Window

For a Kaiser-Bessel window of a particular length N, the parameter β controls the sidelobe height and it affects the sidelobe attenuation of the fourier transform of the window. This parameter also trades off main lobe width against side lobe attenuation [5.20]. The Kaiser-Bessel window in sampled version with β is computed as follows

$$w[n] = \begin{cases} \dfrac{I_0\left(\beta\sqrt{1-\left(\dfrac{2n}{N-1}-1\right)^2}\right)}{I_0(\beta)}, & if \quad 1 \le n \le N \\ 0, otherwise \end{cases} \tag{5.20}$$

Where I_0 is the zeroth order modified Bessel function of the first kind, β is an arbitrary real number that determines the shape of the window, N is the length of the window. The design formula that is used to calculate β parameter value due required a sidelobe level

$$\beta = \begin{cases} 0.1102(\alpha - 8.7) , & \alpha > 50 \\ 0.5842(\alpha - 21)^{0.4} + 0.07886(\alpha - 21) , & 21 \le \alpha \le 50 \\ 0 , & \alpha < 21 \end{cases} \tag{5.21}$$

Where α is sidelobe level in decibels. As β increases, the main lobe width widens and the sidelobe attenuation increases [5.19, 5.20]. For β = 0, the Kaiser-Bessel window is a rectangular window. For β= 5.44, the Kaiser-Bessel window is close to the Hamming window.

Typically, the value of β is in the range from four to eight and for a given parameter, the sidelobe height is fixed with respect to window length. The Kaiser-Bessel window of length 100 for different values of β is plotted in Figure 5.12.

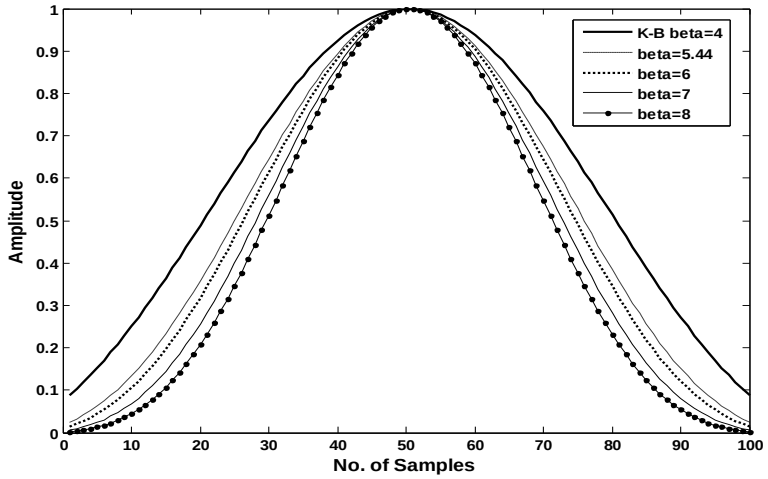

Figure 5.12. Kaiser-Bessel code of length 100 for different β values

For any given window, the signal-to-noise loss (SNR loss) can be calculated by the formula [5.1]

$$SNR_{loss} = \frac{\left(\sum_{n=1}^{N} w[n]\right)^2}{\sum_{n=1}^{N} w[n]^2} \tag{5.22}$$

5.5.3. Simulation Results and Discussion

The Hamming window and Kaiser Bessel windows are applied as sidelobe reduction techniques for P4 code. At the receiver side, the code signal is multiplied with the window coefficients and the weighted code and transmitted one are subjected to autocorrelation.

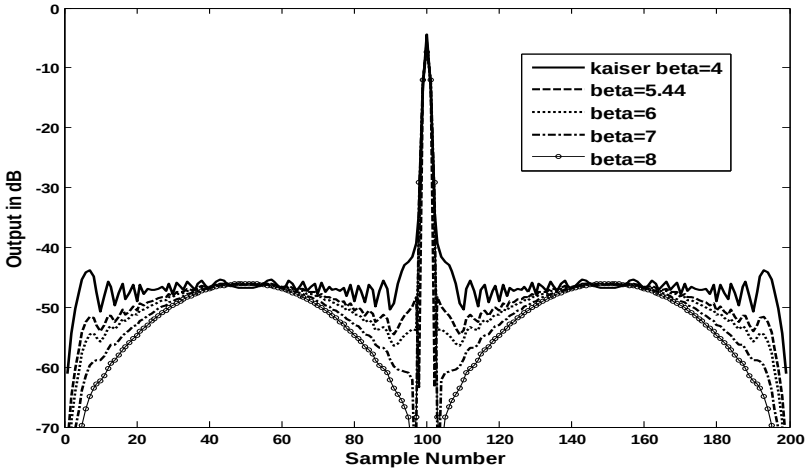

Figure 5.13. Autocorrelation function of P4 signal, N=100, Kaiser-Bessel window for various β parameter value

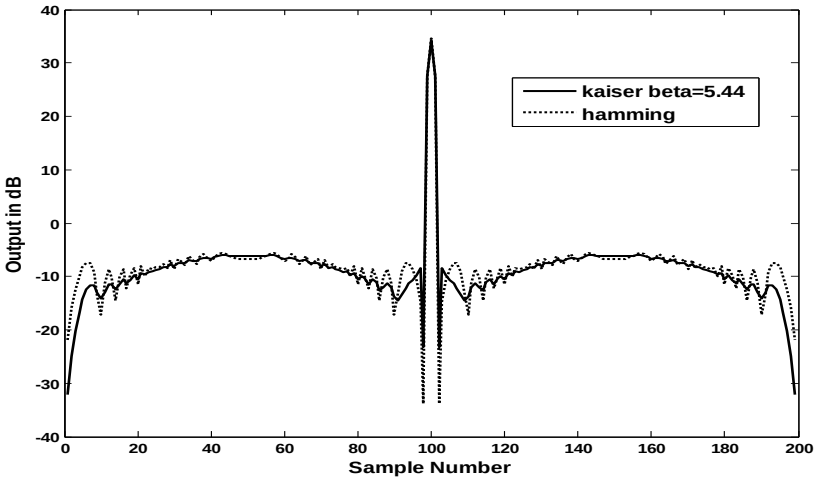

Figure 5.14. ACF of P4 signal, N=100, with Hamming window and Kaiser-Bessel window (β=5.44)

The autocorrelated output using Kaiser Bessel window for different values of β for P4 code of length 100 is given in Figure 5.13. A comparison of ACFs using Hamming window and Kaiser Bessel window of β = 5.44 for 100-element P4 code is given in Figure 5.14. The PSL and ISL values for the same are depicted in Table 5.2.

Table 5.2. Performance for 100 element P4 code

Window name	Peak Sidelobe Level (dB)	Integrated Sidelobe Level (dB)	Weighting SNR loss
Rectangular	-26.32	-12.00	0
Hamming	-40.08	-19.73	-1.37
Kaiser-Bessel β=4	-29.78	-18.29	-0.98
K-B, β=5.44	-40.34	-19.89	-1.52
K-B, β=6	-35.06	-19.72	-1.71
K-B, β=7	-26.19	-18.28	-1.99
K-B, β=8	-21.77	-16.28	-2.26

5.5.3.1. Doppler Properties of P4 weighted Code

The effect of amplitude weighting of Hamming and Kaiser Bessel windows of P4 code under Doppler shift conditions are examined. Figure 5.15(a) shows the ACF of P4 signal for various Doppler shifts, where the one is normalized to the signal bandwidth. Figure 5.15(b) shows the effects of Hamming and Kaiser Bessel windowing techniques under Doppler of -0.05. The PSL and ISL values under Doppler of -0.05 for weighed P4 code are depicted in Table 5.3.

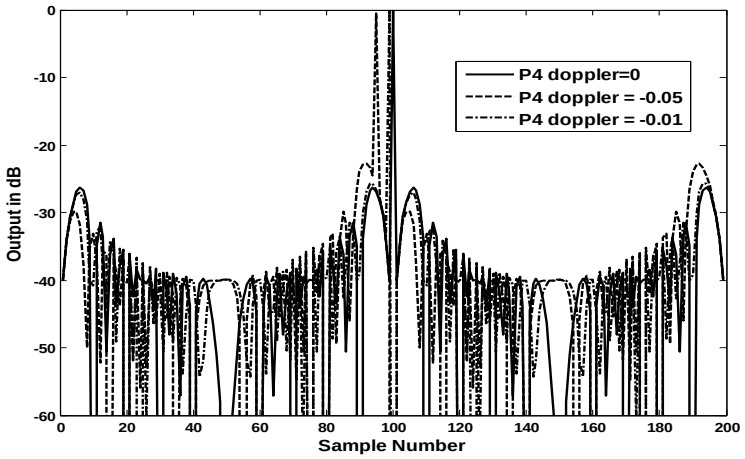

(a)

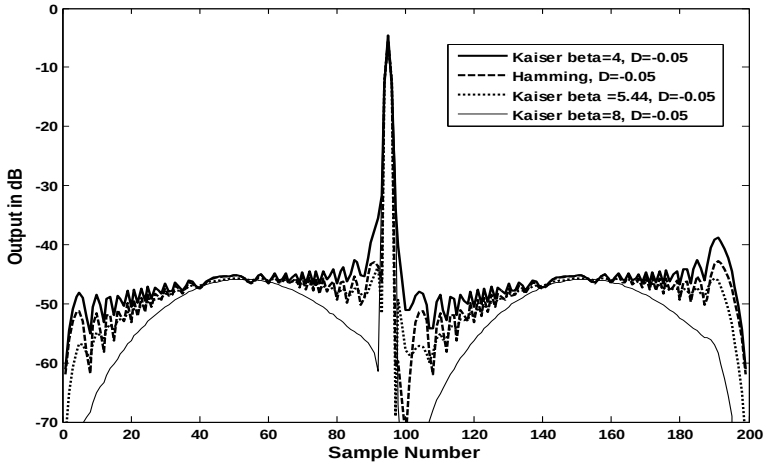

(b)

Figure 5.15. Autocorrelation function of 100-elementP4 signal (a) and weighted P4 code (b) for various windows and Doppler =-0.05

Table 5.3. Performance of p4 weighted code under Doppler=-0.05

Window name	Peak Sidelobe Level (dB)	Integrated Sidelobe Level (dB)
Rectangular	-22.38	-10.66
Hamming	-37.29	-19.01
Kaiser-bessel β=4	-27.14	-17.35
K-B, β=5.44	-37.98	-19.38
K-B, β=8	-21.78	-16.21

5.6. Summary

In this chapter, the Golay complementary codes and polyphase codes are described. The performances of polyphase codes namely Frank, P1, P2, P3, P4 codes, their autocorrelation properties, their phase values and their properties under Doppler shift conditions are discussed. The Single TSSWA and double TSSWA outputs for P4 code are explained in detail and proved that this technique reduces the PSL value. Inorder to reduce the PSL values further, weighting techniques are employed. The Hamming and Kaiser Bessel windowing functions are studied and their effects to P4 code under Doppler of 0 and -0.05 are discussed.

Chapter – 6

Conclusion and Scope of Future Work

6.1. Conclusion

In this thesis, we have presented novel techniques for pulse radar detection. The concepts of pulse compression, phase coded pulse compression and different barker codes are studied. The major aspects for any pulse compression technique are signal to sidelobe ratio performance, noise performance and Doppler tolerance performance. Many techniques were employed to detect a radar pulse which include Adaptive filtering techniques using LMS, RLS, and modified RLS algorithms, multilayered neural network approach and RBF approaches. We proposed the Elman's recurrent neural network for pulse radar detection which gave better results compared to other techniques. There is a scope of futher improvement in all the aspects for most of the applications.

In another chapter, the recurrent RBF is proposed for pulse radar detection to compress the unwanted self-clutter sidelobes. The performance of the RRBF is found to be the best in terms of convergence rate and signal to sidelobe ratio (SSR) for sidelobes reduction over a wide range of SNR. Also, RRBF network is more tolerant to Doppler shift in comparison to other networks like RBF and MLP.

In other chapter, Golay complementary codes and polyphase codes are described. In this study, the performances of polyphase codes namely Frank, P1, P2, P3, P4 codes, their autocorrelation properties, their phase values and their properties under Doppler shift conditions are discussed.

The sidelobe reduction techniques for polyphase codes are presented. The Single TSSWA and double TSSWA outputs for P4 code are explained in detail and proved that this technique reduces the PSL value. In order to reduce the PSL values further, weighting techniques are employed. The Hamming and Kaiser Bessel windowing functions are studied and the performances of both the windows for P4 code are presented. The performance of Kaiser Bessel window depends on β parameter and proper choice of this parameter significantly reduces sidelobe level of compressed P4 signal. Also, this window has an additional advantage of being less sensitive to Doppler shift.

6.2. Scope of Future Work

The work can be extended by improving SSR performance, error convergence, noise performance and doppler shift interference by using the networks trained by evolutionary algorithms. There is a scope of designing a polyphase code which has lower sidelobes and is more Doppler tolerant than the codes discussed in the thesis by using Multiobjective Optimization techniques.

References

Chapter-1

[1.1] Merrill I. Skolnik, *Introduction to radar systems*, McGraw Hill Book Company Inc.,1962.

[1.2] Nadav Levanon, Eli Mozeson, "Radar Signals", 1.st Editon Wiley-Interscience, 2004.

[1.3] Carpentier, Michel H., "Evolution of Pulse Compression in the Radar Field," *Microwave Conference, 1979. 9th European* , vol., no., pp.45-53, 17-20 Sept. 1979

[1.4] Fu, J.S. and Xin Wu, "Sidelobe suppression using adaptive filtering techniques", *in Proc. CIE International Conference on Radar*, pp.788-791, Oct. 2001.

[1.5] B. Zrnic, A. Zejak, A. Petrovic, and I. Simic, "Range sidelobe suppression for pulse compression radars utilizing modified RLS algorithm", *in Proc. IEEE Int. Symp. Spread Spectrum Techniques and Applications*, Vol. 3, pp. 1008-1011, Sep 1998.

[1.6] H. K. Kwan and C. K. Lee, "A neural network approach to pulse radar detection", *IEEE Trans. Aerosp. Electron. Syst.*, vol. 29, pp. 9–21, Jan.1993.

[1.7] D.G. Khairnar, S.N. Merchant and U.B. Desai, "Radial basis neural network for pulse radar detection", *Radar, Sonar & Navigation, IET***,** vol 1**,** pp-8-17, Feb 2007.

[1.8] R. L. Frank, "Polyphase Codes with Good Non periodic Correlation Properties", IEEE Trans. on Information Theory, vol. IT-9, pp. 43-45, Jan. 1963

[1.9] B. L. Lewis, F. F. Kretschmer Jr., "A New Class of Polyphase Pulse Compression Codes and Techniques", IEEE Trans. on Aerospace and Electronic Systems, vol. AES-17, no. 3, pp. 364-372, May 1981

[1.10] B. L. Lewis, F. F. Kretschmer Jr., "Linear Frequency Modulation Derived Polyphase Pulse Compression Codes", IEEE Trans. on Aerospace and Electronic Systems, vol. AES-18, no. 5, pp. 637-641, Sep. 1982

Chapter-2

[2.1] Merrill I. Skolnik, *Introduction to radar systems*, McGraw Hill Book Company Inc.,1962.

[2.2] F.E. Nathanson, J. P. Reilly and M. N. Cohen, *"Radar Design Principles Signal Processing and the Environment"*, 2nd ed. New York: McGraw-Hill, 1999, ch. 1 &8.

[2.3] W. Siebert, "A Radar Detection Philosophy," *IRE Trans.*, vol.IT-2, no. 3, pp. 204-221, Sept. 1956.

[2.4] M.N.Cohen, J.M. Baden, and P. E. Cohen, "Biphase Codes with Minimum Peak Sidelobe," IEEE *International Radar Conf*, 1989, pp. 62-66.

[2.5] Talal Darwich, "*High Resolution Detection Systems using Low Sidelobe Pulse Compression Techniques*", Ph.D. Thesis, University of Louisiana, 2007.

[2.6] Vikas Baghel, "*Multiobjective Optimization — New Formulation and Application to Radar Signal Processing*", M.Tech Thesis, National Institute of Technology, Rourkela, Orissa, India, 2009.

[2.7] B. Widrow and S.D. Sterns, *"Adaptive Signal Processing"*, Prentice-Hall, Inc. Englewood Cliffs, New Jersey, 1985.

[2.8] S. Haykin, "*Adaptive Filter Theory*", 4th edition, Pearson Education Asia, 2002.

[2.9] S. Haykin, "*Neural Networks: A comprehensive foundation*" 2nd Edition, Pearson Education Asia, 2002.

[2.10] B. Zrnic, A. Zejak, A. Petrovic, and I. Simic, "Range sidelobe suppression for pulse compression radars utilizing modified RLS algorithm", *in Proc. IEEE Int. Symp. Spread Spectrum Techniques and Applications*, Vol. 3, pp. 1008-1011, Sep 1998.

[2.11] Satyasai Jagannath Nanda, "*Artificial Immune Systems : Principle, Algorithms and Applications",* M.Tech (R) Thesis, National Institute of Technology, Rourkela, Orissa, India, 2009.

[2.12] Babita Mahji, "*On Applications of New Soft and Evolutionary Computing Techniques to Direct and Inverse Modeling Problems*", Ph.D. Thesis, National Institute of Technology, Rourkela, Orissa, India, 2010.

Chapter-3

[3.1] Merrill I. Skolnik, *Introduction to radar systems*, McGraw Hill Book Company Inc.,1962.

[3.2] F.F. Kretschmer, K.R.Gerlach, 'New radar pulse compression waveforms', *proceedings of 1988 IEEE National*.

[3.3] R. J. Keeler and C.A. Hwang, 'Pulse compression for weather radar', *Radar Conference, 1995., Record of the IEEE 1995 International.*

[3.4] Fu, J.S. and Xin Wu, "Sidelobe suppression using adaptive filtering techniques", *in Proc. CIE International Conference on Radar*, pp.788-791, Oct. 2001.

[3.5] B. Zrnic, A. Zejak, A. Petrovic, and I. Simic, "Range sidelobe suppression for pulse compression radars utilizing modified RLS algorithm", *in Proc. IEEE Int. Symp. Spread Spectrum Techniques and Applications*, Vol. 3, pp. 1008-1011, Sep 1998.

[3.6] H. K. Kwan and C. K. Lee, "A neural network approach to pulse radar detection", *IEEE Trans. Aerosp. Electron. Syst.*, vol. 29, pp. 9–21, Jan.1993.

[3.7] S. Haykin, "*Neural networks, A comprehensive foundation"*, McMillan College publishing Company, New York, 1994.

[3.8] M. T. Haygan, H. B. Demuth, M. Beale, "*Neural Network Design*", Thomson Asia Pte. Ltd , Singapore,2002.

[3.9] Bose N.K., and Liang P., "*Neural Network Fundamentals with Graphs, Algorithms, Applications"*, TMH Publishing Company Ltd, 1998.

[3.10] Lippmann, R.P., "*An Introduction to Computing with Neural Nets"*, Ieee Assp Mag., 1987,4, (2), pp. 422

[3.11] Mikael Boden, "A guide to recurrent neural networks and backpropagation", Nov 2001, Available: www.itee.uq.edu.au/~mikael/papers/rn_dallas.pdf .

[3.12] M.M. Choubassi, H.E. Khoury, C.E. Alagha, J.A. Skaf, and M.A. Al-Alaoui, "Arabic speech recognition using recurrent neural networks", *in Proc. 3rd IEEE International Symposium*, pp. 543–547, 2003.

[3.13] S.F. Toha, M. O. Tokhi, "MLP and Elman recurrent neural network modelling for the TRMS", *7th IEEE International conference on Cybernetic Intelligent System.*, pp. 1-6, sept.2008.

[3.14] Henry C. C. Tan and Liyanage C. De Silva, 'Human Activity Recognition by Head Movement using Elman Network and Neuro-Markovian Hybrids', Nov 2003, http://sprg.massey.ac.nz/ivcnz/Proceedings/IVCNZ_58.pdf.

[3.15] H.D. Griffiths and L.Vinagrae, "Design of low-sidelobe pulse compression waveforms," *Electron Lett.,* vol.30, no.12, pp. 1004- 1005, June 1994.

[3.16] K.D.Rao and G.Sridhar, " Improving performance in pulse radar detection using neural networks.", *IEEE Trans. Aerosp. Electron. Syst.,* vol.31, pp. 1194-1198, July 1995.

[3.17] Ackroyd, M.H., and Ghani, F. 'Optimum mismatch filters for sidelobe suppression', *IEEE Trans. Aerosp. Electron. Syst*., 1973, 9, (2), pp. 214–218

Chapter-4

[4.1] Merrill I. Skolnik, *Introduction to radar systems*, McGraw Hill Book Company Inc.,1962.

[4.2] B. Zrnic, A. Zejak, A. Petrovic, and I. Simic, "Range sidelobe suppression for pulse compression radars utilizing modified RLS algorithm", *in Proc. IEEE Int. Symp. Spread Spectrum Techniques and Applications*, Vol. 3, pp. 1008-1011, Sep 1998.

[4.3] Fu, J.S. and Xin Wu, "Sidelobe suppression using adaptive filtering techniques", *in Proc. CIE International Conference on Radar*, pp.788-791, Oct. 2001.

[4.4] H. K. Kwan and C. K. Lee, "A neural network approach to pulse radar detection", *IEEE Trans. Aerosp. Electron. Syst.*, vol. 29, pp. 9–21, Jan.1993.

[4.5] D.G. Khairnar, S.N. Merchant and U.B. Desai, "Radial basis neural network for pulse radar detection", *Radar, Sonar & Navigation, IET***,** vol 1**,** pp-8-17, Feb 2007.

[4.6] Duh, F.B., Juang, C.F., and Lin, C.T., 'A neural fuzzy network approach to radar pulse compression', *IEEE Geosci. Remote Sens. Letters, 2004*

[4.7] Mudukutore, A.S., Chandrasekar, V., and Keeler, R.J.: 'Pulse compression for weather radars', *IEEE rans. Geosci. Remote Sens.*, vol 36, pp. 125–142, Jan 1998.

[4.8] S. Haykin, *Neural networks: A comprehensive foundation*, McMillan College publishing Company, New York, 1994.

[4.9] R. Bambang, "Active noise cancellation using recurrent radial basis function neural networks", Asia-*Pacific Conference on Circuits and Systems,* vol 2, pp. 231- 26A , 2002.

[4.10] Z. Ryad, R. Daniel, and Z. Noureddine, "The RRBF. Dynamic representation of time in radial basis function network," *in Proceedings of 8th IEEE Int Conf on Emerging Technologies and Factory Automation (ETFA '01)*, vol. 2, pp. 737-740, October 2001.

[4.11] B. Abdelhamid, "Radial Basis Function Nets for Time Series Prediction", *International Journal of Computational Intelligence Systems*, Vol.2, pp. 147-157, June 2009.

[4.12] M. Mimura, N. Hamada, T. Furukawa, "A recurrent RBF network for non-linear channel with time-varying characteristic, *Proc. of IEEE Int. Conf. on Acoustics, Speech, and Signal Processing*, vol 1, pp. 1081- 1084, 2002.

[4.13] G. Hardier, "Recurrent RBF networks for suspension system modeling and wear diagnosis of a damper", *The 1998 IEEE International Joint Conference on Neural Networks Proceedings*, vol. 3, pp.2441-2446, May 1998.

[4.14] G. Hongwei, Y. Weinan, "Color Image Restoration Based on Dynamic Recurrent RBF Neural Network," *Third Int. Conf. on Natural Computation (ICNC 2007)*, vol. 3, pp.123-127, 2007.

[4.15] Chen, S.C., and Grant, P.M., 'Orthogonal least squares learning algorithm for radial basis function networks', *IEEE Trans. Neural Networks*, 1991, 2, (2), pp. 302–309.

[4.16] Bucci, N.J., Owen, H.S., Woodward, K.A., and Hawes, C.M., 'Validation of pulse compression techniques for meteorological functions', *IEEE Trans. Geosci. Remote Sens.*, 1997, 35, pp. 507–523

[4.17] Edde, B., '*Fundamentals of radar*' (IEEE Press, Piscataway, NJ, 2000)

[4.18] Edde, B., '*RADAR principle, technology, applications*' (PTR Prentice Hall, 1993)

Chapter-5

[5.1] Nadav Levanon, Eli Mozeson, "*Radar Signals*", 1.st Editon Wiley-Interscience, 2004.

[5.2] M.G. Parker, K.G. Paterson & C. Tellambura, "Golay Complementary Sequences", in Wiley Encyclopedia of Telecommunications, John G. Proakis, ed., Wiley, 2003

[5.3] S. Searle, S. Howard,"A Novel Polyphase Code for Sidelobe Suppression", Invited Paper, *IEEE Trans. On Waveform Diversity and Design*, 2007.

[5.4] R. L. Frank, "Polyphase Codes with Good Nonperiodic Correlation Properties", *IEEE Trans. on Information Theory*, vol. IT-9, pp. 43-45, Jan. 1963

[5.5] B. L. Lewis, F. F. Kretschmer Jr., "A New Class of Polyphase Pulse Compression Codes and Techniques", IEEE *Trans. on Aerospace and Electronic Systems*, vol. AES-17, no. 3, pp. 364-372, May 1981

[5.6] B. L. Lewis, F. F. Kretschmer Jr., "Linear Frequency Modulation Derived Polyphase Pulse Compression Codes*", IEEE Trans. on Aerospace and Electronic Systems*, vol. AES-18, no. 5, pp. 637-641, Sep. 1982

[5.7] B. L. Lewis, F. F. Kretschmer Jr., W. W. Shelton, "Aspects of Radar Signal Processing", Artech House Inc., MA, 1986

[5.8] B. L. Lewis, "Range-Time-Sidelobe Reduction Technique for FM-Derived Polyphase PC Codes*", IEEE Trans. on Aerospace and Electronic Systems*, vol. AES-29, no. 3, pp. 834-840, July 1993

[5.9] F. F. Kretschmer Jr., L. R. Welch, "Sidelobe Reduction Techniques for Polyphase Pulse Compression Codes", *IEEE International Radar Conference*, pp. 416-421, May 2000.

[5.10] Sato, R., Shinriki, M., "Time sidelobe reduction technique for binary phase coded pulse compression," *Radar Conference, 2000. The Record of the IEEE 2000 International* , vol., no., pp.809-814, 2000

[5.11] Yu Gen-miao, Wu Shun-jun, Luo Yong-jian, "Doppler Properties of Polyphase Pulse Compression Codes under Different Side-lobe Reduction Techniques", *CIE International Conference on Radar*, pp. 524-528, Oct. 2001

[5.12] M. H. Ackroyd, F. Ghani, "Optimum Mismatched Filters for Sidelobe Suppression", *IEEE Trans. on Aerospace and Electronic Systems*, vol. AES- 9, no. 2, pp. 214-218, Mar. 1973

[5.13] W. K Lee, H.D. Griffiths, "Development of modified polyphase P codes with optimum sidelobe characteristics", *IEEE Proc. Radar Sonar Navig*, 151(4), pp. 210–220, Aug 2004

[5.14] R. Sato, I. Sasase, M. Shinriki, "Time sidelobe reduction technique with small S/N loss for binary coded pulse compression", *Proc. Intl. Conf. Radar 2001*, pp. 947–951 (2001)

[5.15] F. F Kretschmer Jr. and B. L. Lewis, "Doppler properties of polyphase pulse compression waveforms*", IEEE Transactions on Aerospace and Electronic System*, Vol.19, No.4, 521-531, May 1983.

[5.16] M. Luszczyk, D. Mucha, "Kaiser-bessel window weighting function for polyphase pulse compression code," *Microwaves, Radar and Wireless Communications, 2008. MIKON 2008. 17th International Conference on* , vol., no., pp.1-4, 19-21 May 2008.

[5.17] Erkan Cankaya," *Use of the Ambiguity Function Technique for Target Detection in Phase Coded Continuous Wave Radar*", M.S. thesis, Middle East Technical University, Dec 2005.

[5.18] Onur Aktop, "*Optimization of Doppler Processing by using Bank of Matched Filters"*, M.S. thesis, Middle East Technical University, Sep 2005.

[5.19] Oppenheim, A.V., and R.W. Schafer, *"Discrete-Time Signal Processing*", Prentice-Hall, 1989, pp. 447-448.

[5.20] Kaiser, J.F., "Nonrecursive Digital Filter Design Using the I0- sinh Window Function," *Proc. 1974 IEEE on Symp. Circuits and Systems*, (April 1974), pp.20-23.

[5.21] Selected Papers in Digital Signal Processing II, IEEE Press, New York, 1975